TROPICAL TROPOPAUSE LAYER

S. Fueglistaler,[1] A. E. Dessler,[2] T. J. Dunkerton,[3] I. Folkins,[4] Q. Fu,[5] and P. W. Mote[3]

Received 4 March 2008; revised 16 September 2008; accepted 14 October 2008; published 17 February 2009.

[1] Observations of temperature, winds, and atmospheric trace gases suggest that the transition from troposphere to stratosphere occurs in a layer, rather than at a sharp ''tropopause.'' In the tropics, this layer is often called the ''tropical tropopause layer'' (TTL). We present an overview of observations in the TTL and discuss the radiative, dynamical, and chemical processes that lead to its time-varying, three-dimensional structure. We present a synthesis definition with a bottom at 150 hPa, 355 K, 14 km (pressure, potential temperature, and altitude) and a top at 70 hPa, 425 K, 18.5 km. Laterally, the TTL is bounded by the position of the subtropical jets. We highlight recent progress in understanding of the TTL but emphasize that a number of processes, notably deep, possibly overshooting convection, remain not well understood. The TTL acts in many ways as a ''gate'' to the stratosphere, and understanding all relevant processes is of great importance for reliable predictions of future stratospheric ozone and climate.

Citation: Fueglistaler, S., A. E. Dessler, T. J. Dunkerton, I. Folkins, Q. Fu, and P. W. Mote (2009), Tropical tropopause layer, *Rev. Geophys.*, *47*, RG1004, doi:10.1029/2008RG000267.

1. INTRODUCTION

[2] The traditional definitions of the troposphere and stratosphere are based on the vertical temperature structure of the atmosphere, with the tropopause either at the temperature minimum (''cold point tropopause'') or at the level where the temperature lapse rate meets a certain criterion (definition by the World Meteorological Organization). Over the past decades it has become clear that the distinction between troposphere and stratosphere may not always be adequately clear and that there is an atmospheric layer that has properties both of the troposphere and the stratosphere. In the tropics, the transition from troposphere to stratosphere may extend over several kilometers vertically, and a number of different definitions and concepts of this tropical tropopause layer (TTL, sometimes also referred to as ''tropical transition layer'') exist in the literature. The TTL is of interest not only because of being the interface between two very different dynamical regimes but also because it acts as a ''gate to the stratosphere'' for atmospheric tracers such as water vapor and so-called very short lived (VSL) substances, which both play an important role for stratospheric chemistry.

[3] This paper examines and discusses observations in the TTL and the processes that contribute to its unique properties. In addition to the mean vertical structure, we also emphasize spatial patterns and examine its variations in longitude, latitude, and season. Our examination of observations and theories emphasizes that the troposphere and stratosphere each have distinct properties and the TTL is by definition the zone where the properties of both troposphere and stratosphere can be observed. Each quantity considered here (temperature variability, ozone, etc.) could by itself conceivably lead to a different definition of the TTL, as in the fable of the blindfolded men describing an elephant. (One feels its tail and reports that the elephant is thin and ropy, one feels the side and reports that it is broad and leathery, etc.) Our purpose here is to integrate these disparate observations into a conceptually simple but theoretically robust definition of the TTL.

[4] Figure 1 shows a schematic of the tropical troposphere and lower stratosphere (Figure 1 (left) shows cloud processes, and Figure 1 (right) shows zonal mean circulation). Tropical deep convection reaches altitudes of 10–15 km. Some convection may reach higher, and very rarely, convection may even penetrate into the stratosphere. At ~200 hPa (350 K, 12.5 km), the meridional temperature gradient reverses sign, which is also the level of the core of the subtropical jet (as expected from thermal wind balance). We set the lower bound of the TTL above the levels of main convective outflow, i.e., at ~150 hPa (355 K, 14 km). Below, air is radiatively cooling (subsiding), and ascent occurs predominantly in moist convection. Above that level, air is radiatively heated under all sky conditions. The level

[1]Department of Applied Mathematics and Theoretical Physics, University of Cambridge, Cambridge, UK.
[2]Department of Atmospheric Sciences, Texas A&M University, College Station, Texas, USA.
[3]NorthWest Research Associates, Redmond, Washington, USA.
[4]Department of Physics and Atmospheric Science, Dalhousie University, Halifax, Nova Scotia, Canada.
[5]Department of Atmospheric Sciences, University of Washington, Seattle, Washington, USA.

8755-1209/09/2008RG000267
Paper number 2008RG000267

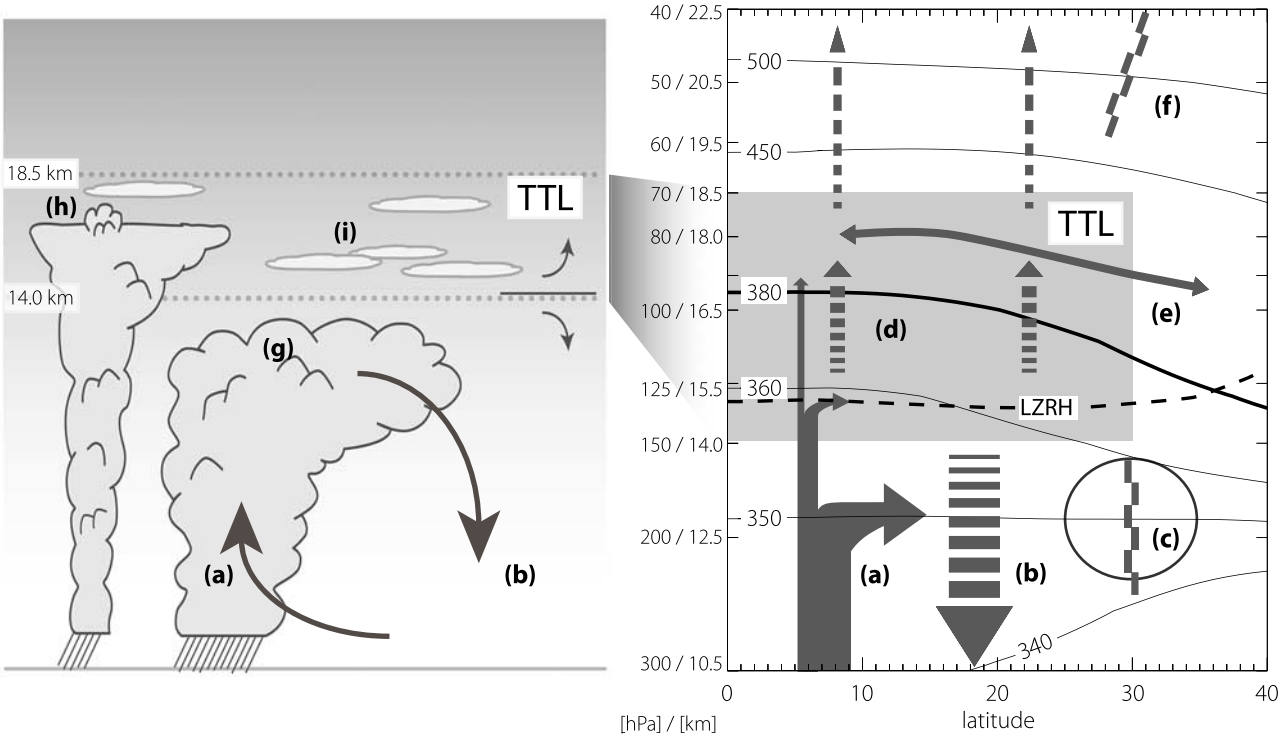

Figure 1. Schematic (left) of cloud processes and transport and (right) of zonal mean circulation. Arrows indicate circulation, black dashed line is clear-sky level of zero net radiative heating (LZRH), and black solid lines show isentropes (in K, based on European Centre for Medium Range Weather Forecasts 40-year reanalysis (ERA-40)). The letter a indicates deep convection: main outflow around 200 hPa, rapid decay of outflow with height in tropical tropopause layer (TTL), and rare penetrations of tropopause. Fast vertical transport of tracers from boundary layer into the TTL. The letter b indicates radiative cooling (subsidence). The letter c indicates subtropical jets, which limit quasi-isentropic exchange between troposphere and stratosphere (transport barrier). The letter d indicates radiative heating, which balances forced diabatic ascent. The letter e indicates rapid meridional transport of tracers and mixing. The letter f indicates the edge of the "tropical pipe," relative isolation of tropics, and stirring over extratropics ("the surf zone"). The letter g indicates deep convective cloud. The letter h indicates the convective core overshooting its level of neutral buoyancy. The letter i indicates ubiquitous optically (and geometrically) thin, horizontally extensive cirrus clouds, often formed in situ. Note that the height-pressure-potential temperature relations shown are based on tropical annual mean temperature fields, with height values rounded to the nearest 0.5 km.

of zero radiative heating (LZRH) under clear-sky conditions is slightly higher, at ~125 hPa (360 K, 15.5 km) as shown by the dashed line in Figure 1 (right). The upper bound of the TTL is set at ~70 hPa (425 K, 18.5 km), and laterally, the TTL is bounded by the position of the underlying subtropical jets (i.e., equatorward of ~30° latitude). In the lower part of the TTL, meridional transport is limited by the large gradients in potential vorticity associated with the subtropical jets [e.g., *Haynes and Shuckburgh*, 2000]. In the upper part of the TTL, rapid horizontal transport to higher latitudes and mixing into the tropics from higher latitudes [e.g., *Volk et al.*, 1996; *Minschwaner et al.*, 1996] is observed. Above the TTL (above 60 hPa, 450 K), the inner tropics become relatively isolated (the "tropical pipe" [*Plumb*, 1996]).

[5] Our definition of the TTL is primarily motivated by the observed large-scale dynamical structures. The horizontal circulation and temperature structure of the TTL are strongly influenced by the distribution of convection in the troposphere, while vertical motion is increasingly dominated by eddy-driven circulations typical of the stratosphere. Rare detrainment of deep convective clouds may occur throughout the TTL and likely has impacts on tracer concentrations, and perhaps the heat budget, of the TTL.

[6] We begin this review (section 2) with an overview of observations of temperature, wind, clouds, and atmospheric trace gases and how these observables show a transition from tropospheric to stratospheric characteristics. (The data sources and a list of acronyms are given in Tables A1–A3 in Appendix A.) Section 3 discusses the dynamical and radiative processes that lead to the observed structure of the TTL and discusses chemical and cloud microphysical processes active in the TTL. Section 3 also provides a brief summary of issues that have been under debate for quite some time; other historical references are given in the individual sections in their context. Section 4 presents the

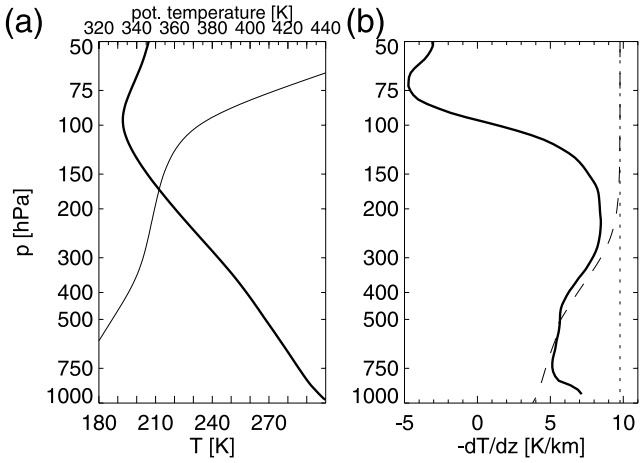

Figure 2. (a) Climatological, annual mean temperature (bold) and potential temperature (thin) profile from Java (7.5°S, 112.5°E). (Data from Southern Hemisphere Additional Ozonesondes (SHADOZ) program [*Thompson et al.*, 2003a] for period 1998–2005.) (b) Corresponding lapse rate (bold). Thin dashed and dotted lines indicate moist and dry adiabatic lapse rates, respectively.

considerations that form the foundation for the definition of the TTL as given above. Finally, section 5 provides a brief outlook.

2. OBSERVATIONS

[7] Over the past 2 decades, large efforts have been undertaken to improve data coverage in the TTL with the necessary vertical, spatial, and temporal resolution required to accurately characterize the transitional character of the TTL. Here we use assimilated meteorological fields, remote sensing, and in situ measurements to provide short overviews of temperature, wind, water vapor, clouds, ozone, and water isotopologues. Further, we briefly discuss carbon monoxide, nitrogen species, and radon. Other tracers, for example, CO_2, are discussed in the context of their relevance for the TTL.

2.1. Temperature

[8] Temperature is a fundamental state variable of the atmosphere, linking atmospheric motion, clouds, radiation, (moist) convection, and chemical reactions. Temperatures around the tropical tropopause came into focus also because of their role in determining stratospheric water vapor (discussed in sections 2.4 and 3.6 below). Horizontal and seasonal variations in TTL temperature and thermodynamic properties are broadly associated with the distribution of convection and large-scale upward motion. However, we emphasize that there is no simple correspondence of, for example, boundary layer equivalent potential temperature and cold point potential temperature.

[9] Temperature observations with high vertical resolution from radiosondes have been available since the 1950s. Since the 1970s, spaceborne measurements have provided layer average temperatures with global and high temporal coverage but poor vertical resolution. In more recent years, a wealth of spaceborne instruments have provided near-global coverage of temperature in three dimensions. In addition, the development of global data assimilation methods at the U.S. National Centers for Environmental Prediction (NCEP) and the European Centre for Medium-Range Weather Forecasts (ECMWF) provides a tool for integrating observations into a global, dynamically consistent, and temporally complete data set. Here we use radiosonde data and ECMWF 40-year reanalysis (ERA-40) data [*Uppala et al.*, 2005] to describe the structure and variability of temperature. (For descriptions based on radiosondes, see, e.g., *Kiladis et al.* [2001] and *Seidel et al.* [2001]; for descriptions based on GPS data, see, e.g., *Schmidt et al.* [2004] and *Randel and Wu* [2005].)

[10] Figure 2a shows an annual mean temperature profile over Java (7.5°S, 112.5°E) from the Southern Hemisphere Additional Ozonesondes (SHADOZ) program [*Thompson et al.*, 2003a]. The cold point tropopause is situated around 90 hPa, 190 K (∼17 km, 380 K). The observed lapse rate ($-dT/dz$, where T is temperature and z is height; Figure 2b) follows closely the moist adiabatic (dashed line) from ∼750 to ∼200 hPa. Very low temperatures above 200 hPa lead to minute water vapor pressures, such that the moist adiabate approaches the dry adiabate. The observed temperature profile begins to depart from moist adiabatic around 300–200 hPa, implying that increasingly stable stratification begins several kilometers below the tropopause. The lapse rate maximizes in the layer 300–200 hPa and shows a characteristic minimum (i.e., a maximum in static stability) near 70 hPa.

[11] Figure 3a shows the annual, zonal mean temperature structure in the upper troposphere/lower stratosphere from the tropics to midlatitudes. Meridional temperature gradients are very small in the tropics but increase substantially over the subtropics. The latent heat release associated with frequent deep convection in the tropics forces tropical temperatures up to a level of ∼350 K to be higher than those over the subtropics. Above 350 K, the meridional temperature gradient over the subtropics reverses its sign, and the tropics now have, remarkably, lower temperatures than the subtropics and midlatitudes. This change of sign is also reflected by the differing curvatures of the 340 and 360 K isentropes.

[12] Figure 4a shows the climatological mean annual cycle of tropical mean temperatures. Upper tropospheric temperatures show little seasonal variation, but there is a pronounced annual cycle around the tropopause and in the lower stratosphere, with lowest temperatures during boreal winter and highest temperatures during boreal summer. This layer of coherent temperature variations on a seasonal time scale extends from ∼125 to ∼25 hPa. Above that, temperature variations are controlled by the stratospheric semiannual oscillation [*Reed*, 1962] that shows little or no correlation with temperatures at tropopause levels. Below 125 hPa, tropical mean temperature variations are associated with the seasonal migration of the Intertropical Convergence

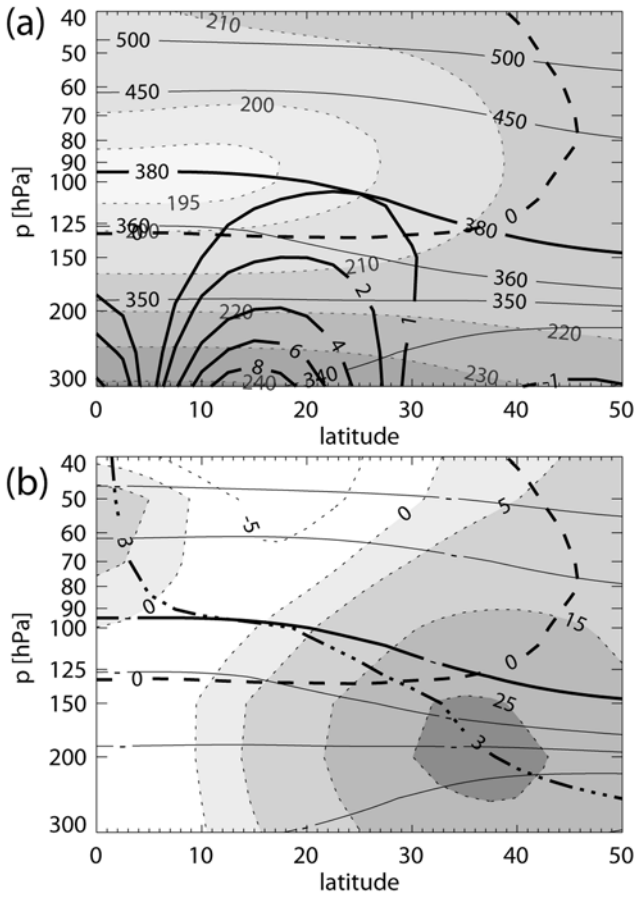

Figure 3. Zonal mean, annual mean Northern Hemispheric structure of (a) temperature (in K, grey scale, dotted lines), potential temperature (in K, solid lines), level of zero clear-sky radiative heating (LZRH, dashed line), and stream function (in 10^{10} kg/s, bold line) and (b) potential temperature and LZRH as in Figure 3a, potential vorticity 3 PVU (dash-dot-dot-dotted line), and zonal wind (in m/s, grey scale, dotted lines). All data from ERA-40 [*Uppala et al.*, 2005].

Zone (ITCZ), and the monsoons and are weakly anticorrelated (not shown) with tropopause temperatures.

[13] Figure 4b shows the meridional structure of the amplitude of the annual cycle in temperatures from ERA-40 data. Consistent with the first description by *Reed and Vlcek* [1969], the annual cycle in temperature in the tropics shows a maximum at 80 hPa of ~8 K (peak to peak). In ERA-40 the region of maximum amplitude of the tropical annual cycle is shifted toward the Northern Hemisphere, but the amplitude of the annual cycle is more symmetric about the equator than in the original analysis of *Reed and Vlcek* [1969]. The annual character of temporal variability of tropical mean temperatures around the tropopause seems at odds with the seasonal ITCZ migration (crossing the equator twice per year) and has prompted different explanations (see discussions in sections 3.2, 3.4, and 3.7). The large amplitudes on the poleward sides of the subtropics may be explained, at least in part, as a consequence of the north/south displacement with seasons of the position of large meridional temperature gradients over the subtropics. Accordingly, the phase of the annual cycle over the northern subtropics is shifted by 6 months compared to that over the southern subtropics.

[14] Interannual variability of temperatures in the TTL, typically of order 1 K at the tropopause [e.g., *Randel et al.*, 2004], may arise because of the El Niño–Southern Oscillation (ENSO), volcanic eruptions, and temperature perturbations induced by the quasi-biennial oscillation (QBO). While there is consensus that the lower stratosphere is cooling [*Ramaswamy et al.*, 2001], temperature trends at tropopause levels have larger uncertainties, and we only touch on the subject in section 5.

[15] Figure 5 shows maps of monthly mean temperature from ERA-40 reanalysis data at 150, 100, and 70 hPa for January and July 2000 (ozone and water vapor will be

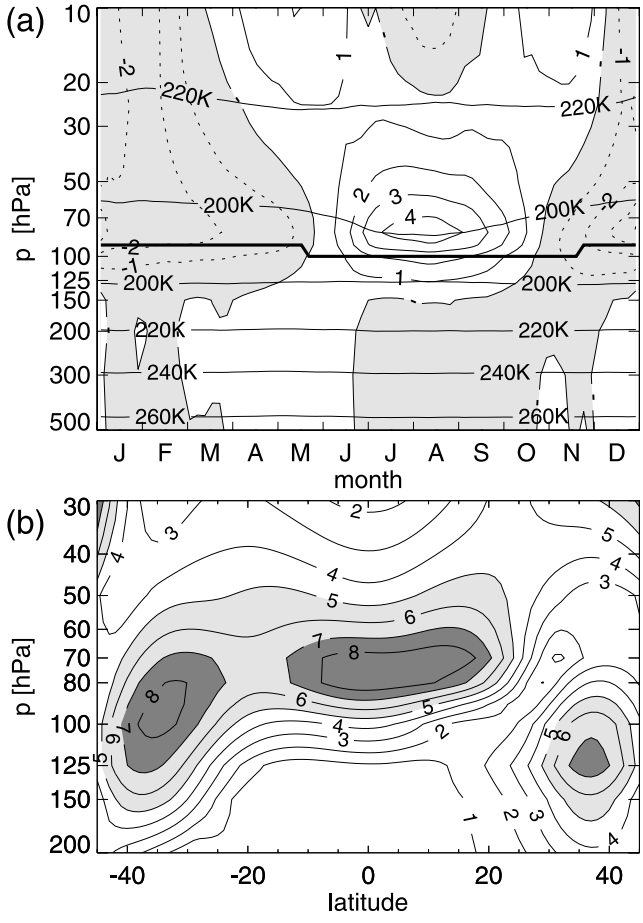

Figure 4. (a) Climatological tropical (10°S–10°N) mean annual cycle of temperatures (black lines, as labeled) and temperature anomalies from annual mean profile in K (contour lines, negative values grey shaded and dashed contour lines). The thick black line shows the pressure level of the cold point tropopause as represented in ERA-40. (b) Latitudinal structure of peak to peak difference of annual cycle of zonal mean temperatures (contour lines, values exceeding 5 and 7 K light and dark grey shaded, respectively). All data from ERA-40 [*Uppala et al.*, 2005].

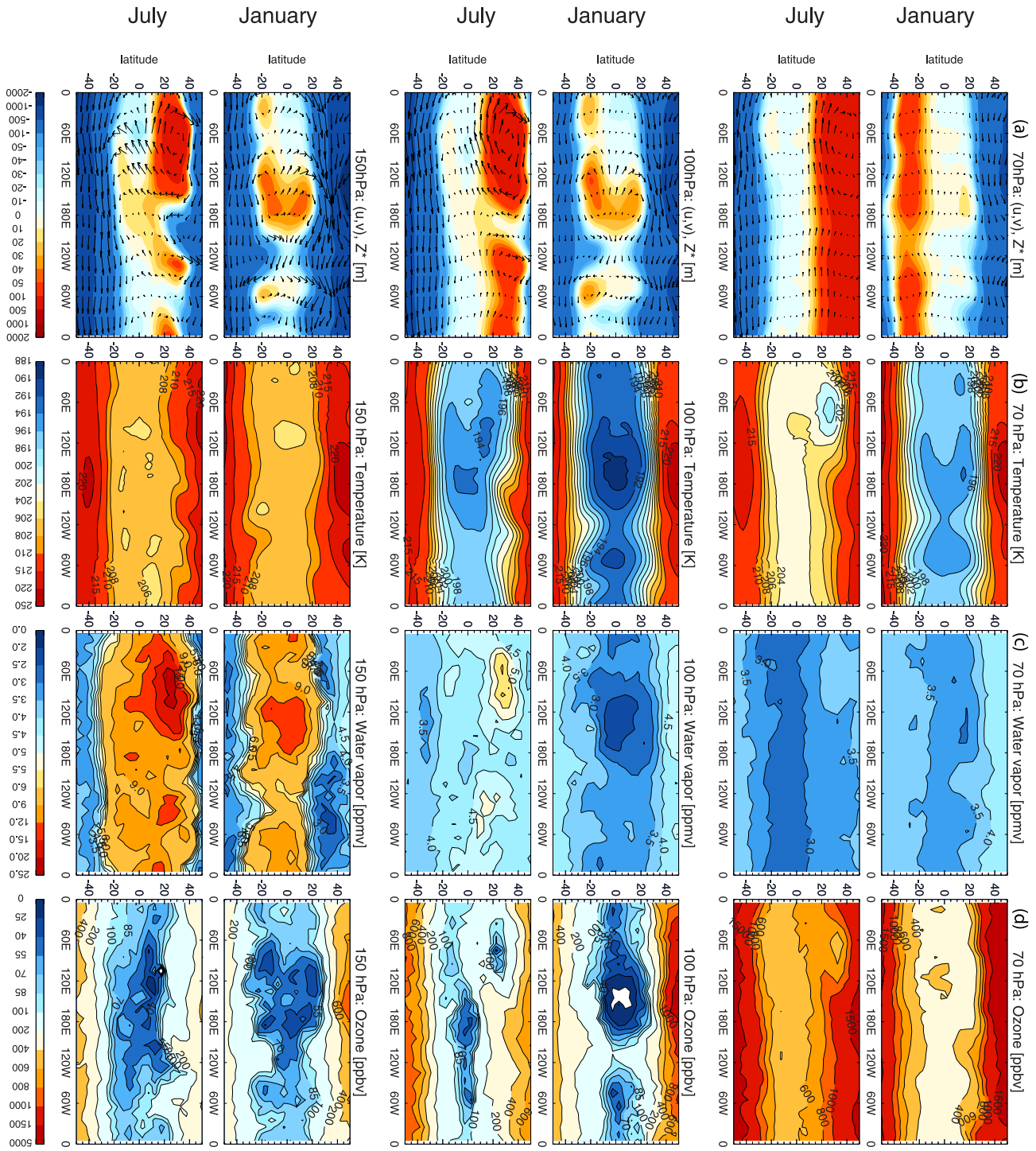

Figure 5. Maps on 150, 100, and 70 hPa of January and July mean fields. (a) Wind (vector field, arbitrarily scaled for best visual representation of flow) and geopotential height anomaly relative to 10°S–10°N mean (ERA-40, averaged 1990–2000); (b) temperature (ERA-40 [*Uppala et al.*, 2005], averaged 1990–2000); (c) water vapor (Microwave Limb Sounder (MLS)/Aura data v2.2 [*Read et al.*, 2007], January and July 2006); and (d) ozone (MLS/Aura data v2.2 [*Froidevaux et al.*, 2006], January and July 2006). Note irregular contour increments to capture full dynamic range of data; white areas indicate no valid data.

discussed in sections 2.3 and 2.4). The maps show steep meridional temperature gradients over the subtropics, with a steeper gradient over the corresponding winter hemisphere. Within the tropics, monthly mean temperatures at 150 hPa show little spatial variability. From 150 to 70 hPa, temperatures show characteristic spatial patterns, with maximum temperature anomalies around the tropopause (see 100 hPa temperature fields of Figure 5) of up to 5 K compared to the

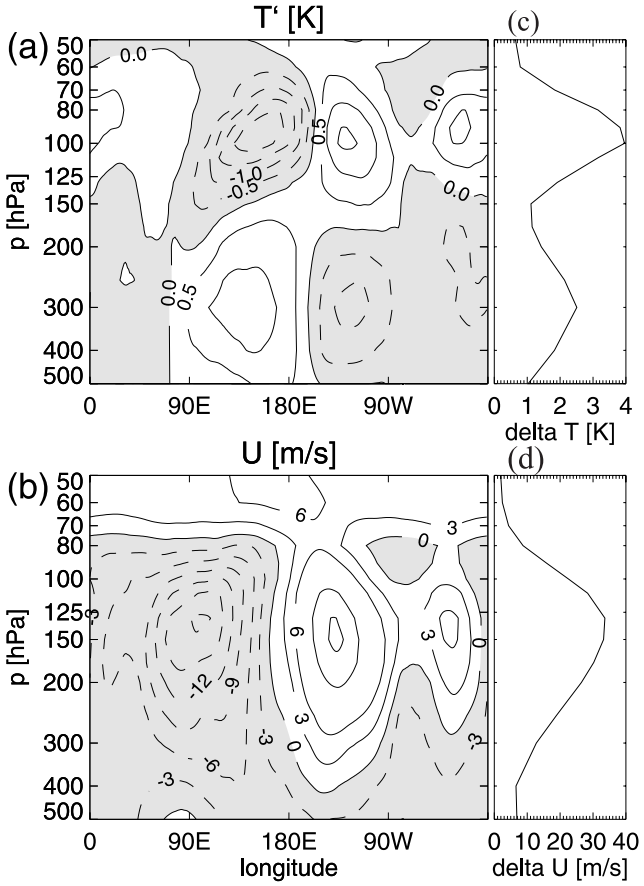

Figure 6. Annual mean (year 2000) zonal structure of inner tropical (10°S–10°N) (a) zonal temperature anomalies (in K) and (b) zonal wind (in m/s, positive values correspond to eastward winds). (c and d) Profiles of zonal amplitude (maximum – minimum). Note that structures persist throughout the year but that averaging over a year reduces their amplitudes. (Individual months may have zonal temperature anomalies up to a factor two higher.) All data from European Centre for Medium-Range Weather Forecasts (ECMWF) ERA interim [*Simmons et al.*, 2006].

zonal mean during boreal winter and somewhat smaller differences during boreal summer. During boreal winter, minimum temperatures are found over equatorial South America and, in particular, over the western tropical Pacific with the characteristic westward extensions north and south of the equator. During boreal summer, a somewhat similar picture emerges that shows, however, a clear northward displacement over the Indian/Southeast Asian monsoon region. These patterns extend up to ~70 hPa and eventually vanish with height.

[16] Figure 6a shows the annual mean structure of inner tropical (10°S–10°N) zonal temperature anomalies in longitude/pressure, and Figure 6c shows the profile of the maximum temperature difference on pressure levels. The quadrupole structure centered near the dateline persists throughout the year, and its amplitude on a monthly mean basis, in particular for boreal winter months, is up to a factor of two larger than in the annual mean (not shown). Figure 6a shows upper tropospheric anomalies arising from convection over the western Pacific warm pool and subsidence over the eastern Pacific (the Walker circulation, see section 3.3). The amplitude of zonal temperature variability shows a local minimum at ~150 hPa and a maximum at tropopause levels. Note the eastward tilt with height of the cold anomaly in the TTL west of the dateline. The vertical structure of the amplitude of the time mean, zonal temperature structure (Figure 6c) above 150 hPa resembles that of the seasonal cycle but decays more rapidly with height.

2.2. Wind

[17] The circulation, and hence also the horizontal wind field, plays an important role for transporting tracers in the TTL, and, like temperature, reveals important information about the dynamics governing the TTL. Figure 3b shows the annual, zonal mean zonal wind in the region of interest (note that Figure 3b shows only the Northern Hemisphere; Southern Hemisphere winds are similar). Figure 3b shows generally weak zonal mean, zonal winds in the inner tropics up to the tropopause. Above, the inner tropical zonal wind is strongly modulated by the stratospheric QBO (for a review, see *Baldwin et al.* [2001]), and the data shown reflect the particular phase of the QBO for the year 2000. The vacillations of equatorial zonal wind associated with the QBO are attenuated below ~50 hPa but are still discernible in the upper part of the TTL [e.g., *Giorgetta and Bengtsson*, 1999; *Randel et al.*, 2000; *Fueglistaler and Haynes*, 2005]. In the upper tropical troposphere, the zonal mean zero-wind line is located at ~10° latitude. Between ~125 and 50 hPa, the zero-wind line bends poleward to ~30° latitude. Figure 3b further shows strong westerlies over the subtropics with a maximum at ~200 hPa (corresponding to 350 K potential temperature). Note that the maximum is, following thermal wind balance, tied to the isentrope with zero meridional gradient.

[18] Figure 6b shows the annual mean zonal wind in the inner tropics (10°S–10°N). Figure 6b shows that the aforementioned weak zonal mean, zonal wind in the TTL in fact is the residual of two regions with strong zonal winds of opposite directions. East of the dateline, strong westerlies prevail in the layer from 400 hPa to about the tropopause that form the upper branch of the so-called "Walker circulation" over the Pacific. West of the dateline, easterlies prevail, also known as the "equatorial easterlies." This dipole structure is tightly coupled to the distribution of deep convection (further discussed in section 3.3). Figure 6d shows that the maximum amplitude of zonal wind anomalies (here defined as maximum minus minimum) is situated at ~150 hPa, which is also about the level where zonal temperature anomalies reverse sign (Figure 6a).

[19] Figure 5 shows maps of winds (together with geopotential height anomalies) in the tropics at 150, 100, and 70 hPa. The wind field in the TTL is dominated by huge, quasi-stationary anticylones, with the boreal winter pattern being highly symmetric about the equator. During boreal summer, two anticylones are observed over the Northern Hemisphere, and only weak counterparts are observed over

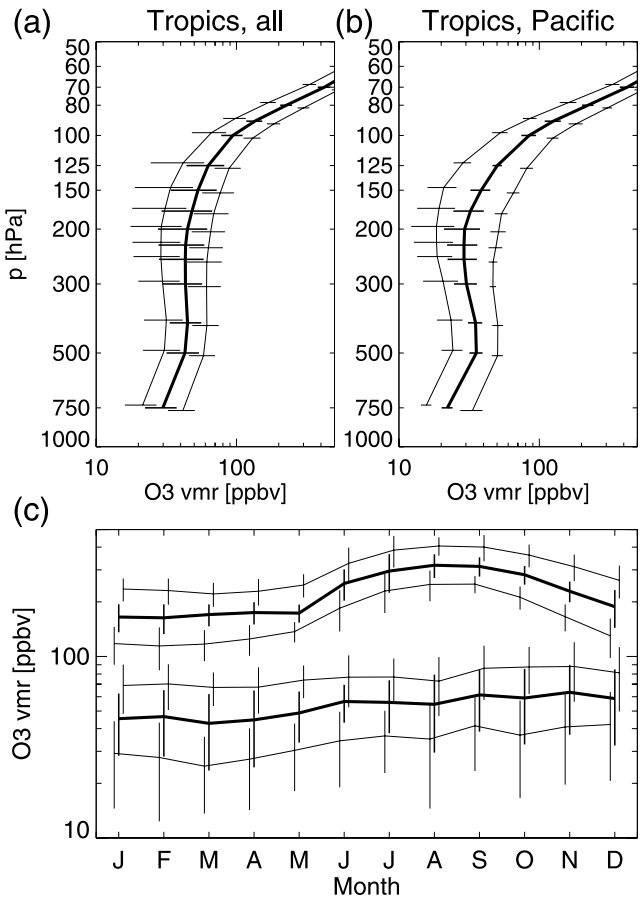

Figure 7. Climatological (period 1998–2005), annual mean ozone profiles from SHADOZ [*Thompson et al.*, 2003a]: (a) all tropical stations and (b) tropical Pacific stations. (c) Climatological annual cycle at 150 and 80 hPa (all tropical stations). Black solid line indicates 50th percentile, and thin black lines indicate 10th and 90th percentiles. Bars show standard deviation of each percentile between the following stations: Ascension (8°S, 14°W), Java (7.5°S, 112.5°E), Fiji (18°S, 178.5°E), Kuala Lumpur (2.5°N, 101.5°E), Malindi (3°S, 40°E), Nairobi (1.5°S, 37°E), Natal (5.5°S, 35.5°W), Paramaribo (6°N, 55°W), Samoa (14°S, 170.5°E), and San Cristobal (1°S, 89.5°W). Fiji, Samoa, and San Cristobal are also used for subgroup tropical Pacific.

the Southern Hemisphere. Figure 5 also shows that particularly during boreal winter, over the eastern Pacific the wind field shows a pronounced narrowing of the Westerlies toward the equator which may affect Rossby wave propagation (further discussed in section 3.3).

2.3. Ozone

[20] Ozone is far more abundant in the stratosphere than in the troposphere and hence is a tracer frequently used in studies of troposphere-stratosphere exchange in general and for studies of the TTL in particular [e.g., *Folkins et al.*, 1999]. In the free troposphere, ozone is photochemically produced, with enhanced production rates in polluted surface air and in air exposed to biomass burning. In the tropical boundary layer, in particular over the oceans, net ozone destruction occurs [e.g., *Jacob et al.*, 1996]. In the stratosphere, ozone is rapidly photochemically produced, and concentrations increase strongly with height in the lower stratosphere. Ozone concentrations in the TTL are controlled by the complex interplay of horizontal and vertical transport, including troposphere-stratosphere exchange, and by in situ chemical reactions (further discussed in section 3.5).

[21] Figure 7 shows tropical, climatological annual mean distributions (percentiles) of ozone concentrations as determined from SHADOZ [*Thompson et al.*, 2003a] measurements (see caption of Figure 7 for list of stations; note bias toward Southern Hemisphere). It has been previously noted that tropical ozone concentrations show large spatial and temporal variability [e.g., *Thompson et al.*, 2003a] that make a general overview a difficult task. This is readily seen in the substantial variability among the stations as revealed by the standard deviation of the percentiles shown in Figure 7, and due care should be used when interpreting these averaged concentrations as representative for the whole tropics.

[22] An interesting feature of the ozone profile particularly over sites in the tropical Pacific (Figure 7b) is the prevalence of an "S shape," with concentrations slightly increasing from near-surface to the free troposphere, followed by a weak local minimum around 200 hPa, interpreted as a consequence of convective detrainment of ozone-poor low-level air [e.g., *Lawrence et al.*, 1999; *Folkins et al.*, 2002]. Above, concentrations strongly increase to stratospheric values. *Folkins et al.* [1999] examined ozone profiles over Samoa (14°S) and found that the sharp increase in mean ozone at 14 km coincided with increases in the lapse rate of both temperature and equivalent potential temperature.

[23] Tropical tropospheric and total ozone tends to be higher from the Atlantic to the Indian Ocean than over the western and central Pacific during all seasons [*Fishman et al.*, 1990; *Shiotani*, 1992; *Thompson et al.*, 2003b] (a distribution sometimes also called "wave one" pattern). Figure 5 shows maps of ozone concentrations at 150, 100, and 70 hPa from Microwave Limb Sounder/Aura [*Froidevaux et al.*, 2006]. The observed spatial structure and temporal variability reflects in part tropospheric patterns but also transport and the spatiotemporal distribution of ozone sources and sinks (see section 3.5).

[24] Figure 7c shows the seasonality of the SHADOZ tropical mean ozone concentrations at 150 and 80 hPa. At 150 hPa, these ozone concentrations show only weak seasonality, with slightly elevated concentrations during late boreal fall, a seasonal pattern typical also for tropical tropospheric ozone concentrations [*Thompson et al.*, 2003b]. At tropopause levels (80 hPa), Figure 7 shows a strong annual cycle [*Logan*, 1999; *Folkins et al.*, 2006; *Randel et al.*, 2007] with a maximum during boreal summer, in phase with that of temperatures, such that annual variations of ozone concentrations evaluated on isentropes (not shown) are substantially smaller.

2.4. Water Vapor

[25] Water vapor is one of the key tracers for troposphere-stratosphere exchange that led *Brewer* [1949] to deduce that air enters the stratosphere primarily across the tropical tropopause. Despite its low abundance, stratospheric water vapor plays important roles in the radiative budget of the stratosphere [e.g., *Forster and Shine*, 1999] and stratospheric chemistry as the primary source for HO_x and in the activation of chlorine on polar stratospheric clouds (PSCs) that leads to ozone destruction [*Solomon et al.*, 1986]. Hence, the processes that control water vapor in the TTL (discussed in section 3.6) are of importance to the global climate system and have provided much of the motivation for research on the TTL.

[26] The phase changes of water, from vapor to liquid or ice, are so strongly controlled by temperature that in the tropics the average concentration of water vapor drops by four orders of magnitude from the surface to the tropical tropopause. Reliable water vapor measurements at the low concentrations found near the tropopause remain a challenging task. Observations from in situ measurements, restricted in location and time to special campaigns, are available from balloon-borne frostpoint hygrometers, airborne Lyman-Alpha, and tunable diode laser instruments. Global coverage is provided by spaceborne remote sensing instruments operating with microwave emissions or occultation techniques. A major problem of water vapor observations, in particular also for interpretation of relative humidity, is that relatively large biases between instruments [*Kley et al.*, 2000] remain unresolved to date. To remedy the situation, discrepancies between instruments are currently investigated within the Water Vapor Instrument Test and Intercomparison (AquaVIT) project [*Peter et al.*, 2008].

[27] Figure 8a shows annual mean, tropical water vapor concentration profiles from 200 to 50 hPa. The increase of water vapor concentrations above the minimum at tropopause levels is due to in-mixing of stratospherically older air masses with increased water concentrations from oxidized methane and to a lesser degree due to in situ methane oxidation. Figure 8b shows the annual cycle of tropical water vapor mixing ratios, with highest values in boreal autumn, and a distinct upward propagation of maxima and minima from the tropopause. The seasonal cycle of temperatures around the tropopause yields a corresponding seasonal cycle in saturation mixing ratios of air at entry into the stratosphere, which is then advected upward leading to tilted stripes when viewed as a time-height cross section (the "atmospheric tape recorder" [*Mote et al.*, 1995, 1996; *Weinstock et al.*, 1995], see also section 3.6). The ascent rate of water vapor concentrations allows the deduction of

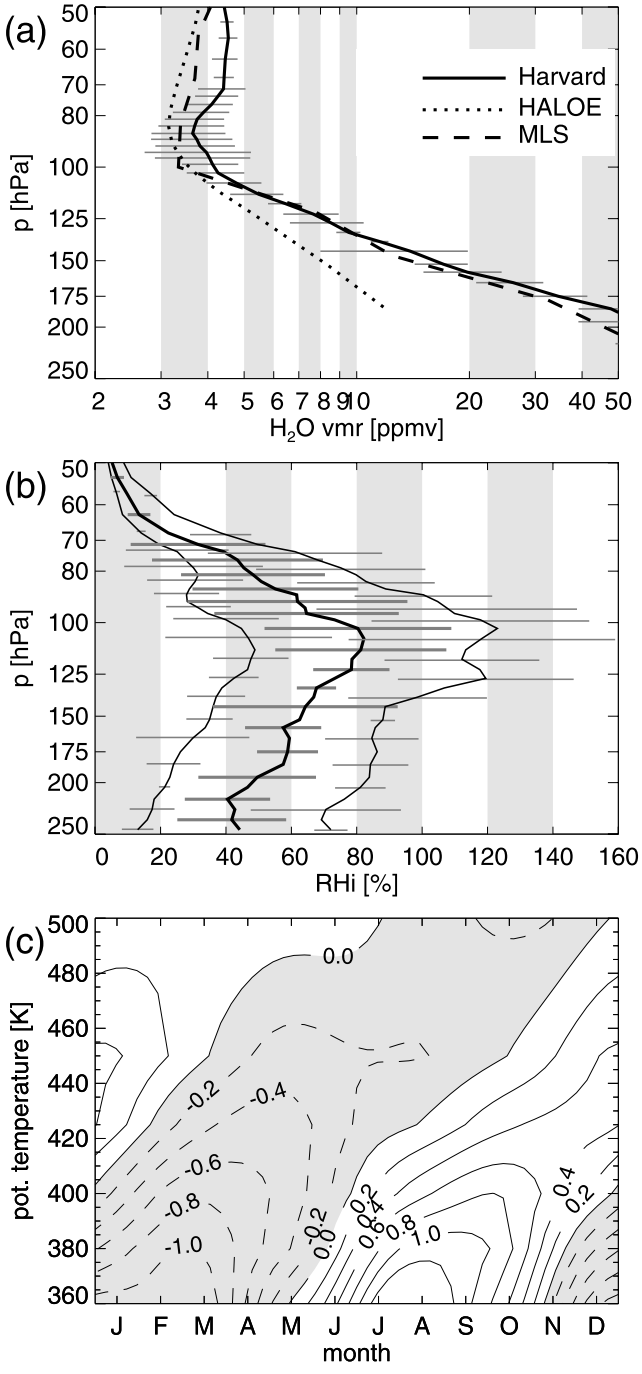

Figure 8. (a) Tropical annual mean water vapor profiles from Halogen Occultation Experiment (HALOE) [*Russell et al.*, 1993] and MLS/UARS [*Read et al.*, 2004] and from the Harvard in situ Lyman-Alpha instrument [*Weinstock et al.*, 1995] (all data 20°S–20°N). Horizontal bars indicate intercampaign (campaigns used are ACCENT, ASHOE-MESA, CEPEX, PRE-AVE, STEP, and STRAT; see Table A3) standard deviation of mean profiles for in situ observations. (b) Profiles of relative humidity over ice (RHi) from Harvard in situ measurements (20°S–20°N) (10th, 50th, and 90th percentiles averaged over all measurement campaigns). Horizontal bars indicate intercampaign standard deviation of each percentile. (c) HALOE [*Russell et al.*, 1993] climatological mean seasonal cycle of tropical water vapor concentration anomalies from annual mean profile (in ppmv, negative values grey shaded; annual mean profile as shown in Figure 8a, dotted line). Data evaluated on isentropes.

mean ascent rates [*Mote et al.*, 1996], as well as seasonal and QBO-related variations [*Niwano et al.*, 2003].

[28] At tropopause and adjacent stratospheric levels, the signal of the time-varying entry mixing ratio spreads to the high latitudes within ~2 months [*McCormick et al.*, 1993; *Hintsa et al.*, 1994; *Randel et al.*, 2001]. During boreal winter, transport processes are thought to be responsible for shifting minimum concentrations to regions north of the equator [*Gettelman et al.*, 2002a], and during boreal summer the Indian/Southeast Asian monsoon leads to exceptionally high water vapor concentrations north of the equator (see Figure 5). Consequently, the maxima in seasonal variation are found north of the equator [e.g., *Randel et al.*, 1998]. Similar to the seasonal variations of entry mixing ratios, interannual variation can be traced both meridionally and vertically [e.g., *Randel et al.*, 2004].

[29] The net efficacy of dehydration during ascent into the stratosphere may be estimated from measurements of the stratospheric hydrogen budget (being the sum of entry mixing ratios of molecular hydrogen, methane, and water vapor, with the first two terms generally well known). Typically, mean entry mixing ratios lie between 3.5 and 4 ppmv [e.g., *Engel et al.*, 1996; *Dessler and Kim*, 1999; *Michelsen et al.*, 2000]. The seasonal variation of entry mixing ratios (estimated from near tropopause level measurements) ranges from ~2.5 ppmv during January/February to ~4.5 ppmv during September/October [e.g., *Randel et al.*, 2001; *Fueglistaler et al.*, 2005]. Interannual variations of entry mixing ratios are of order 0.5 ppmv [*Randel et al.*, 2001; *Fueglistaler et al.*, 2005] for the 1990s and early 2000s, with some observations suggesting a considerable trend in entry mixing ratios over the past 50 years or so [*Rosenlof et al.*, 2001]. A fairly sudden drop of entry mixing ratios of 0.2–0.5 ppmv occurred around the years 2000/2001 [*Randel et al.*, 2006; *Scherer et al.*, 2008].

[30] Figure 8c shows relative humidity (over ice, RHi) profiles in the TTL obtained from in situ observations (see also summary provided by *Jensen et al.* [2001]). Due care should be used when interpreting RHi in the TTL, as it strongly depends on the accuracy of both temperature and water vapor measurements. The following features, however, appear to be fairly robust. In the upper troposphere, the median relative humidity increases from 20 to 40% at 500 hPa (lower estimate based on GPS data [*Sherwood et al.*, 2006]; higher estimate based on radiosondes [*Folkins and Martin*, 2005]) to 40–50% at 200 hPa, as might be expected in a layer of general subsidence that is periodically moistened by convective detrainment. With increasing height, however, RHi increases and shows a maximum (with frequent supersaturation) in the TTL, qualitatively consistent with the idea that from the LZRH upward, air rises but temperature still decreases up to the tropopause, so that air stays close to saturation.

[31] Up to ~150 hPa, the spatial and temporal patterns of water vapor concentrations largely follow that of deep convection [e.g., *Newell et al.*, 1996], with higher concentrations in convectively influenced regions (see Figure 5). In the TTL, minima in water vapor concentrations are found generally in regions of low temperature anomalies, such as above the western Pacific warm pool (see Figure 5).

2.5. Clouds

[32] Clouds are important for the TTL because of their impact on radiation and because their presence (or absence) indicates the activity of convection and in situ condensation. Furthermore, clouds in the TTL have unique properties related to the increasingly stable stratification and little water vapor available for condensation. In particular, widespread layers of cirrus are commonly observed in the TTL, much more commonly than in the tropical troposphere, and may be optically quite thin, even "subvisual" (optical depth < 0.03 [*Sassen and Cho*, 1992]) and may contain as little as 40 ppbv water in the condensed phase [*Peter et al.*, 2003].

[33] Clouds associated with convection include the deep convective cloud itself, a deep and often horizontally extensive anvil cloud, and occasionally a thin Pileus cloud that may show signatures of mixing with air masses of the convective core [*Garrett et al.*, 2004]. Cirrus clouds are more common in the TTL than convective clouds and form either as remnants of convective anvil clouds [e.g., *Dessler and Yang*, 2003] or in situ, with somewhat different shapes and structure [*Pfister et al.*, 2001]. It is estimated that about half of tropical cirrus clouds formed in situ, and the other half formed from remnants of deep convection [*Massie et al.*, 2002; *Luo and Rossow*, 2004]. Generally high relative humidity and small particle sizes with low fall speeds due to very limited available water vapor [*Jensen et al.*, 1996a; *Luo et al.*, 2003] are factors favoring longer cloud persistence in the TTL than elsewhere. The radiative heating of the clouds may also lead to diabatic uplift of the cloud layer ("cloud lofting" [*Jensen et al.*, 1996b]) or drive a local circulation that brings sufficient water vapor to sustain the cloud [*Sherwood*, 1999]. A stabilization of the cloud layer may arise in cases where both upwelling and temperature decrease with height [*Luo et al.*, 2003], which may also help to explain how optically thin clouds with very little ice water content can exist on a time scale of a day and extend over hundreds of kilometers despite being in a thermodynamically delicate state (a small warming would immediately lead to complete evaporation, while a cooling would induce particle growth and rapid sedimentation).

[34] Reliable characterization of cloud properties in the TTL from observations remains a major challenge. Different sensors are sensitive to different particle sizes, have different viewing geometry, and have different spatial and diurnal coverage.

[35] Radar data from the Tropical Rainfall Measuring Mission (TRMM) allow detection of maximum heights where graupel still can be observed (the radar is sensitive only to large particles (>O(100) microns) and has a detection limit of ≈17 dBz). *Liu and Zipser* [2005] found for 5 years of data that 1.3% of tropical convective systems surpass the 14 km level and 0.1% surpass the 380 K (~17 km) level. About 0.2% of the convective systems as observed by TRMM penetrate the local tropopause (as defined using NCEP reanalyses). Ground-based cloud

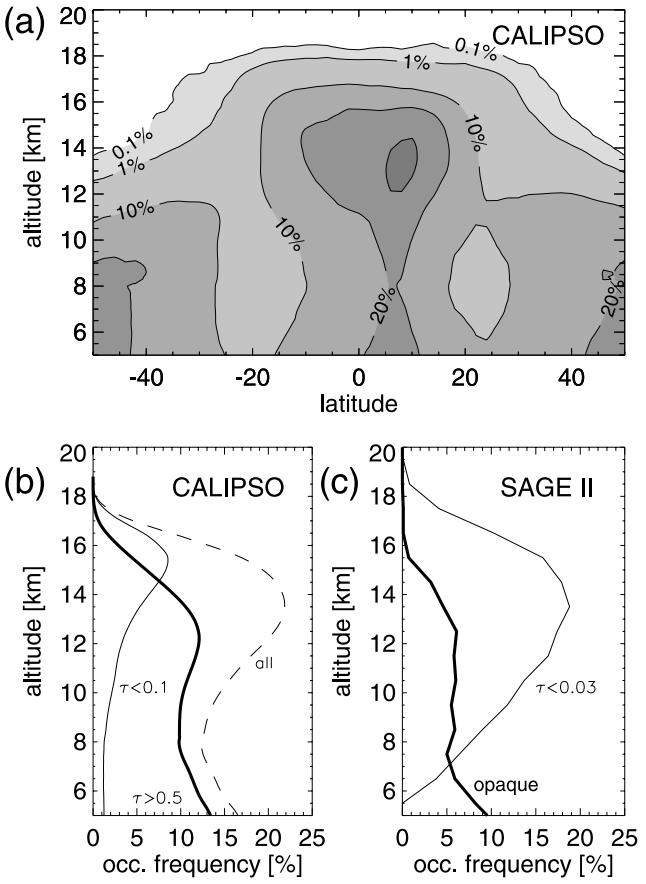

Figure 9. (a) Zonal mean cloud occurrence frequency (data for June 2006 to February 2007). (b) Profiles of 20°S–20°N cloud occurrence frequency for $\tau < 0.1$ (thin line), $\tau > 0.5$ (thick line), and all (dashed line) clouds. Data for Figures 9a and 9b are from Cloud-Aerosol Lidar and Infrared Pathfinder Satellite Observation (CALIPSO) [*Winker et al.*, 2007], adapted from *Fu et al.* [2007]. (c) Profiles (10°S–10°N) of cloud occurrence frequency from Stratospheric Aerosol and Gas Experiment (SAGE II) for optically thick (thick line) and subvisual cirrus (thin line). (Updated from *Wang et al.* [1996].)

radars may be used to study optically thicker clouds [e.g., *Hollars et al.*, 2004], but they miss the optically thin cirrus clouds in the TTL.

[36] Other approaches include nadir-viewing near-infrared (Moderate Resolution Imaging Spectroradiometer [*Dessler and Yang*, 2003; *Mote and Frey*, 2006]), limb-viewing infrared (CRISTA [*Spang et al.*, 2002] and Cryogenic Limb Array Etalon Spectrometer [*Sandor et al.*, 2000]), solar occultation (Stratospheric Aerosol and Gas Experiment (SAGE II) [*Wang et al.*, 1996] and Halogen Occultation Experiment (HALOE) [*Hervig and McHugh*, 1999]), and microwave [*Hong et al.*, 2005] sensors. Thermal imagery provides cloud top height estimates from International Satellite Cloud Climatology Project (ISCCP) [e.g., *Luo and Rossow*, 2004], advanced very high resolution radiometer [*Katagiri and Nakajima*, 2004], and Atmospheric Infrared Sounder [*Kahn et al.*, 2005], to name a few. *Gettelman et al.* [2002b] present a comprehensive compilation of statistics on cloud top frequency as a function of altitude using 11 μm brightness temperatures from 0.5 × 0.5° global cloud imagery. Cloud frequency drops sharply with increasing altitude, but ~0.5% of clouds penetrate the local tropopause, with highest frequency at roughly 12°S in February and 11°N in August. Cloud top heights derived from thermal imagery are found to suffer from a systematic low bias [*Sherwood et al.*, 2004] and miss the highest parts of convective clouds because of the relatively low spatial resolution.

[37] Lidar observations from the ground [e.g., *Immler and Schrems*, 2002] or aircraft [e.g., *Newell et al.*, 1996; *Peter et al.*, 2003] are sensitive also to optically thin clouds, but the presence of optically thick clouds frequently attenuates the lidar beam. The spaceborne lidar data provided by Lidar In-space Technology Experiment [*Winker and Trepte*, 1998]; Ice, Cloud, and Land Elevation Satellite (ICESat)/Geoscience Laser Altimeter System (GLAS); and Cloud-Aerosol Lidar and Infrared Pathfinder Satellite Observation (CALIPSO) have provided a new view of the cloud heights in the TTL. A limitation of data from lidar on satellites with a polar orbit is their limited temporal resolution. For example, CALIPSO crosses the equator only at 0130 and 1330 local time, but convection often has a well-defined diurnal cycle. *Dessler et al.* [2006] find in ICESat/GLAS lidar data 0.34% of optically thick and 3.1% of optically thin clouds (defined as those that the lidar can penetrate) above the average level (377.5 K potential temperature) of the tropopause.

[38] Figure 9a shows zonal mean cloud occurrence frequency determined from CALIPSO averaged over the period June 2006 to February 2007. Figure 9a shows maximum cloud occurrence between 12 and 15 km and ~10°N, consistent with the mean position of the ITCZ and the level of maximum convective outflow. Figure 9b shows the tropical mean (20°S–20°N) cloud occurrence profiles for optically thin ($\tau < 0.1$), for optically thicker ($\tau > 0.5$), and for all cloud. Up to the main convective outflow level, clouds are predominantly optically thicker, whereas above (i.e., in the TTL) they are predominantly optically thin. Total cloud fractions between 20°S and 20°N are ~0.05% at 18.5 km, 0.5% at 18.0 km, and 5% at 17.0 km [*Fu et al.*, 2007]. Figure 9c shows cloud occurrence frequency of opaque and subvisible cirrus obtained from SAGE II averaged between 10°S and 10°N. The differences to the CALIPSO profiles are in part a consequence of different thresholds for optical depths and the narrower latitude belt and in part due to differences in viewing geometry and sensitivity (SAGE II is very sensitive even to thinnest clouds).

2.6. Isotopologues

[39] About 0.03% of atmospheric water vapor consists of deuterated water (HDO), and ~0.2% consists of $H_2^{18}O$. These isotopologues have a lower vapor pressure than H_2O. Consequently, they tend to preferentially condense which can be used to deduce information about dehydration processes.

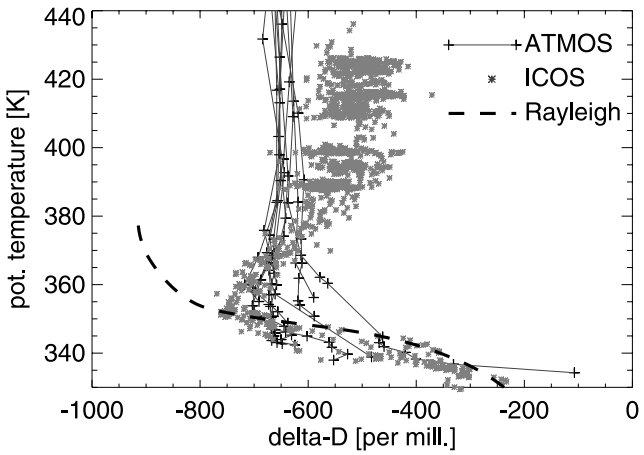

Figure 10. Measurements of δD in the TTL. Atmospheric Trace Molecule Spectroscopy (ATMOS) (11 profiles, November 1994, data courtesy *Kuang et al.* [2003], tangent point height converted to potential temperatures based on UK Met Office analysis data). Harvard in situ measurements by integrated cavity output spectroscopy (Integrated Cavity Output Spectroscopy (ICOS), data from three descents into San Jose/Costa Rice in February 2006, data courtesy T. Hanisco). Rayleigh fractionation curve based on typical tropical temperature profile, initialized in boundary layer.

[40] Observations of water isotopologues in the TTL are available from remote sensing instruments as well as from in situ instruments on high flying aircraft. Most of the measurements that have been made are of HDO, and we will focus on that isotopologue here.

[41] Measurements of HDO in the midstratosphere allow the deduction of the annual mean HDO content of air at entry into the stratosphere δD_e by subtracting the contributions from methane oxidation. Fundamentally, δD is a measure of the abundance of HDO relative to that of H_2O, normalized by the ratio observed in sea water: $\delta D \equiv \frac{(D/H)_{\text{sample}}}{(D/H)_{\text{std}}} \times 1000$ where the standard refers to "standard mean ocean water." A value of 0‰ means that the ratio is equal to that of sea water, while -500‰ means that the ratio in the sample is only half that of the ratio in sea water, and a value of -1000‰ means that the sample contains no HDO. Measurements yield $\delta D_e = -670 \pm 80$‰ [*Moyer et al.*, 1996], $\delta D_e = -679 \pm 20$‰ [*Johnson et al.*, 2001], and $\delta D_e = -653 + 24/-25$‰ [*McCarthy et al.*, 2004].

[42] *Kuang et al.* [2003] show tropical profiles of HDO from Atmospheric Trace Molecule Spectroscopy (ATMOS) measurements [*Gunson et al.*, 1996] that show fairly constant values of $\delta D \approx -650$‰ from ~11 km upward and hence virtually no correlation with water vapor concentration. *Webster and Heymsfield* [2003] show in situ measurements of δD obtained in the boreal summer subtropics that have much larger variability below the tropopause than the ATMOS data. Newer in situ measurements (T. Hanisco et al., personal communication, 2007) show less scatter than the data of Webster and Heymsfield but reveal more structure in the vertical than the ATMOS profiles. Solar occultation Fourier transform infrared measurements from the Mark IV balloon (J. Notholt et al., Transport of water through the tropopause studied from its isotopic composition, submitted to *Nature Geoscience*, 2009) show a correlation of δD_e with water entry mixing ratio with a slope in agreement with expectations based on temperature-dependent Rayleigh fractionation (a theoretical limit derived by assuming that condensation occurs under thermodynamic equilibrium conditions and that the condensate thus formed is instantaneously removed).

[43] Figure 10 shows the ATMOS profiles and the in situ measurements by the Integrated Cavity Output Spectroscopy (ICOS) instrument from three descents into San Jose (Costa Rica) during February 2006. These observations show a minimum in δD at ~355 K, i.e., at the base of the TTL, and less depletion in the stratosphere. ICOS measurements from other flights show less isotopic depletion around 355 K than those shown in Figure 10 (T. Hanisco, personal communication, 2007), which may be related to convection (see section 3.6). Figure 10 also shows δD predicted by a Rayleigh fractionation process along a typical tropical temperature profile. While the differences in δD measurements between instruments need to be resolved in order to allow interpretation, it is clear that all measurements show substantially more HDO in the stratosphere than expected from Rayleigh fractionation. Implications of the δD observations for the water vapor budget of the TTL will be discussed in section 3.6.

2.7. Other Trace Constituents

2.7.1. Carbon Monoxide

[44] The dominant source of CO to the TTL is transport from the troposphere (local photochemical steady state concentrations from methane oxidation would be an order of magnitude smaller than observed). Because the chemical lifetime of CO is comparable with dynamical time scales in the TTL, it has often been used to help quantify convective transport in the TTL (see section 3.4).

[45] Measurements of CO on the 147 and 100 hPa surfaces have recently become available from the Aura Microwave Limb Sounder [*Filipiak et al.*, 2005]. These measurements demonstrate that CO concentrations exhibit substantial geographic variability and have a seasonal cycle in the TTL and lower stratosphere. This cycle is probably due to some combination of seasonal variations in biomass burning, convective outflow, and upwelling [*Schoeberl et al.*, 2006; *Folkins et al.*, 2006; *Randel et al.*, 2007]. Figure 11a shows a tropical annual mean CO profile generated from solar occultation measurements by the Atmospheric Chemistry Experiment–Fourier Transform Spectrometer [*Bernath et al.*, 2005]. The observed CO mixing ratio is ~80 ppbv throughout the upper troposphere but sharply decreases starting at the bottom of the TTL to ~40 ppbv at tropopause level (17 km) and even lower values in the stratosphere.

2.7.2. Nitrogen Species

[46] The concentration of nitrogen oxides is of interest because of its important role in atmospheric chemistry,

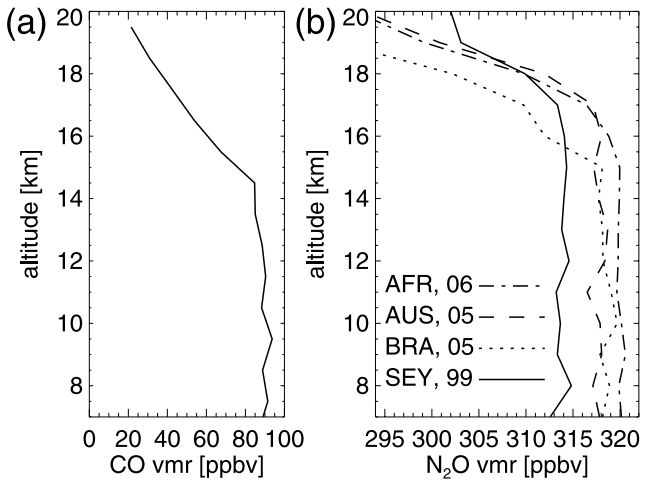

Figure 11. (a) Annual, tropical mean profile of carbon monoxide from the Atmospheric Chemistry Experiment–Fourier Transform Spectrometer [*Bernath et al.*, 2005]. (b) Profiles of nitrous oxide (N_2O) from in situ measurements (averages of campaigns). Solid indicates APE-THESEO, Seychelles, February/March 1999; dotted indicates TROCCINOX, Brazil, February 2005; dashed indicates SCOUT-Tropical, Darwin, Australia, November/December 2005; and dash-dotted indicates SCOUT/AMMA, Africa, August 2006 (see Table A3). Data courtesy C. M. Volk.

particularly also for ozone production and destruction [*Crutzen*, 1974]. Commonly, nitrogen oxides are grouped into NO_x (being the sum of reactive nitrogen species NO and NO_2) and NO_y (being the sum of all reactive odd nitrogen or fixed nitrogen except for the very stable N_2O). Measurements of NO_x at 100 hPa from the HALOE instrument show enhanced NO_x over the continents, presumably arising from convective detrainment of NO_x generated by lightning [*Park et al.*, 2004]. The generally higher values observed by the HALOE instrument (NO_x in the range of 500–800 pptv [*Park et al.*, 2004]) compared with the in situ observations from the Airborne Southern Hemisphere Ozone Experiment/Measurements for Assessing the Effects of Stratospheric Aircraft (ASHOE/MAESA) and Stratospheric Tracers of Atmospheric Transport (STRAT) campaigns (NO concentrations of ~300 pptv [*Folkins*, 2002]) may reflect sampling biases of the aircraft campaigns toward the tropical Pacific.

[47] N_2O is a tracer of interest because it is destroyed by $O(^1D)$ only at altitudes well above the tropopause. N_2O depleted air therefore contains some stratospherically older (order years) air. The profiles of N_2O measured over the Indian Ocean, northern Australia, Brazil, and Africa shown in Figure 11b show constant tropospheric concentrations and a well-defined decrease from the tropopause upward. These profiles suggest that in-mixing of stratospherically older air masses (with low N_2O concentrations) is rare below the tropopause. Because of the subtropical location, the observations over southern Brazil show a decrease at lower altitudes.

2.7.3. Radon

[48] Radon has a source in Earth's crust and experiences rapid radioactive decay with a half life of 3.8 days [*Kritz et al.*, 1993] and hence is an ideal tracer to estimate the transport time scale from the boundary layer to the tropopause. Over land, typical atmospheric activity rates in the boundary layer are 100–200 picocuries per standard cubic meters (pCi/scm), whereas values near the tropopause are on the order of 1 pCi/scm [*Kritz et al.*, 1993], implying transport time scales on the order of 20 days (see summary of time scales in section 3.4). During the Stratosphere-Troposphere Exchange Project (STEP) field campaign near Darwin (Australia), *Kritz et al.* [1993] observed radon activity of ~20 pCi/scm at ~15 km altitude in the cirrus shield of a tropical cyclone, in which the surface source air was presumably a mixture of high-radon land surface air and low-radon ocean air. More typical upper tropospheric measurements during several STEP flights were ~2–4 pCi/scm up to 17 km altitude. Flights in the stratosphere or in the upper troposphere away from convection almost never detected radon activity.

[49] Observations of radon, however, are so rare that it is not possible to generate summary profiles or spatial distributions. What the STEP radon measurements demonstrate is that convection can strongly influence the composition of the TTL up to ~17 km in a highly convective region and time of year.

3. THEORY

[50] We begin the section with the description of atmospheric radiation (section 3.1) because the interaction of solar and infrared radiation with the trace constituents of the atmosphere provides the backdrop against which eddy-driven circulations and convection occur. Next, we provide short descriptions of the stratospheric circulation (section 3.2) and of the tropospheric Hadley, Walker, and monsoon circulations (section 3.3). Convection plays several integral roles in these tropospheric circulations, and section 3.4 discusses its direct impact on the TTL. Chemical reactions (section 3.5) in and near the TTL alter the composition of the air and thereby influence the local radiative balance and the concentration of key substances in the stratosphere, including those that lead to ozone depletion. Issues of dehydration have been central to many aspects of research in the TTL and are discussed in section 3.6. Finally, section 3.7 briefly summarizes the long-standing debate around the roles of large-scale dynamical processes and (mesoscale) moist convection.

3.1. Radiation

[51] Radiative heating rates in the TTL provide important information on the troposphere-to-stratosphere transport. They are, however, a diagnosed quantity and by themselves do not allow direct conclusions on the processes governing the circulation. In the tropical troposphere, temperatures are generally higher than the radiative equilibrium temperature

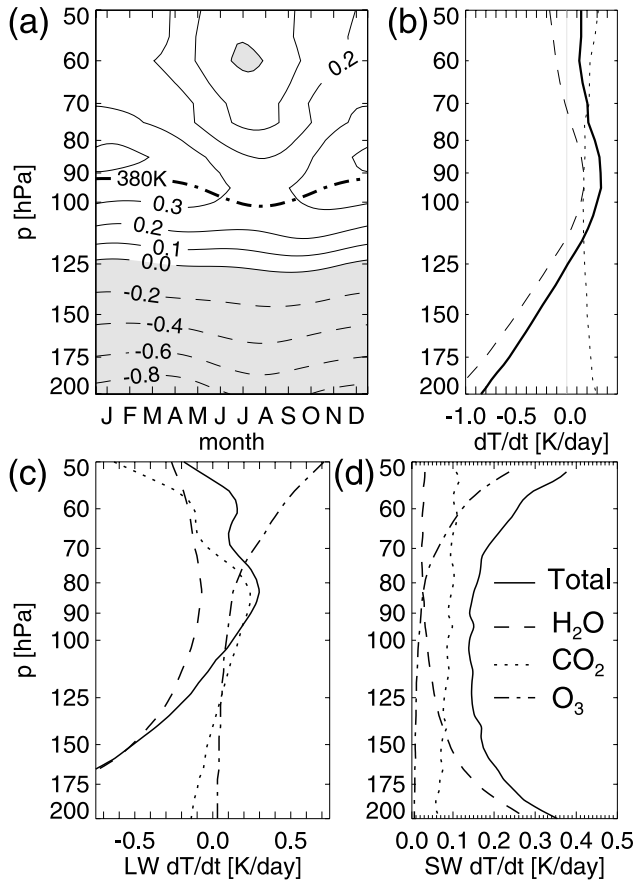

Figure 12. Clear-sky radiative heating rates. (a) Climatological mean annual cycle at tropical SHADOZ stations (calculated with an updated version of the Fu-Liou radiative transfer code). Dash-dotted line shows 380 K isentrope for reference. (b) Corresponding annual mean total (solid) and longwave (dashed) and shortwave (dotted) radiative heating rates. (c) Longwave and (d) shortwave radiative heating rates of typical tropical profile separated to contributions from ozone (dash-dotted), water vapor (dashed), and carbon dioxide (dotted). Data adapted from *Gettelman et al.* [2004a].

($T_{Q=0}$). $T_{Q=0}$ is the temperature at which the radiative heating rate is zero (i.e., emission equals absorption) and may be determined by allowing relaxation of temperature toward radiative equilibrium of the entire profile or of a layer only. Here we refer to the latter which is frequently used in studies of the dynamics of a dry atmosphere. The radiative heating rate Q then is approximated as "Newtonian cooling":

$$Q = -k_{\mathrm{rad}} \cdot \left(T - T_{Q=0}\right), \tag{1}$$

where T and $T_{Q=0}$ are the actual and radiative equilibrium temperatures, respectively, and k_{rad} is the inverse of the radiative relaxation time $\tau_{\mathrm{rad}} = 1/k_{\mathrm{rad}}$. In the troposphere, radiative heating rates are negative (cooling), and temperatures are above the radiative equilibrium temperature. For the tropics as a whole, the radiative loss of energy is largely balanced by the release of latent heat in moist convection. In the stratosphere, latent heat release is negligible. Diabatic ascent in low latitudes and diabatic descent at higher latitudes are balanced by radiative heating and cooling at low and high latitudes, respectively (see Figure 1, label d). Correspondingly, stratospheric temperatures at low latitudes are below the radiative equilibrium temperature, and we observe in the tropics a transition from radiative cooling (in the troposphere) to radiative heating (in the stratosphere).

[52] Figure 12 shows results of radiative transfer calculations (using an updated version of the radiative transfer code by *Fu and Liou* [1992]) for clear-sky conditions using tropical temperature and tracer profiles obtained from the SHADOZ program. Figure 12a shows the seasonal cycle, and Figure 12b shows the corresponding annual mean of longwave, shortwave, and total radiative heating rates. In agreement with previous studies [e.g., *Folkins et al.*, 1999; *Sherwood*, 2000; *Folkins*, 2002; *Gettelman et al.*, 2004a; *Fueglistaler and Fu*, 2006] and the calculations from the ECMWF model shown in Figure 3, the level of net zero clear-sky radiative heating (LZRH, i.e., where $T \equiv T_{Q=0}$) is located at ~125 hPa (corresponding to ~15.5 km or 360 K potential temperature) and shows little variation with season. The heating rates show a local maximum around tropopause levels, with a pronounced annual cycle.

[53] In addition to seasonal variations, radiative heating rates in the TTL show geographical variability associated with temperature and ozone variability and with the geographical distribution of clouds. In the stratosphere, the latitudinal structure of radiative heating rates is also strongly affected by the QBO, and the profiles shown in Figure 12 may not be seen as means over the entire latitudinal belt of upwelling. However, the altitude of the clear-sky LZRH shows little variation in the tropics [*Gettelman et al.*, 2004a].

[54] Figures 12c and 12d show the contributions to the radiative heating rates from water vapor, carbon dioxide, and ozone (see *Gettelman et al.* [2004a] for discussion of CH_4, N_2O, and chlorofluorocarbons). In the troposphere, the radiative balance is dominated by shortwave absorption and longwave emission of water vapor. In the TTL, the extremely low temperatures severely limit the concentration of water vapor and hence also its interaction with radiation. Throughout the TTL, water vapor emits more longwave radiation than it absorbs, and the magnitude of the net longwave component is larger than that of shortwave absorption. The net contribution to radiative heating from ozone is positive throughout the TTL, with a larger contribution from longwave absorption than shortwave absorption [see also *Fu and Liou*, 1992]. The contribution from carbon dioxide shortwave absorption is fairly constant in the TTL, whereas its longwave component, which is generally cooling in the rest of the atmosphere, shows quite large net heating in the TTL.

[55] Calculations of the radiative relaxation time τ_{rad} yield a maximum at tropopause levels because of the low temperatures there (emission scales with temperature to the fourth power). Values for τ_{rad} reported in the literature range

from τ_{rad} = 15–30 days [*Newman and Rosenfield*, 1997; *Hartmann et al.*, 2001] to $\tau_{rad} \approx$ 100 days [*Kiehl and Solomon*, 1986; *Randel et al.*, 2002]. The differences in τ_{rad} probably arise from using different temperature and tracer profiles. Also, the radiative relaxation time depends on the vertical scale of the temperature perturbation (it is roughly inversely proportional to the square root of vertical wave number of the temperature perturbation [*Fels*, 1982; *Bresser et al.*, 1995]). Because of the long radiative relaxation time scale in the TTL, changes in dynamic upwelling must be accounted for by large changes in temperature, which provides a reasonable explanation why the amplitude of the seasonal cycle of temperature (see section 2.1) peaks at tropopause levels [*Randel et al.*, 2002] (see also section 3.2).

[56] The low abundance of radiatively active tracers in the TTL further allows other absorbers, in particular the abundant thin cirrus clouds (see Figure 1, label i, and section 2.5), to become important in the radiative budget. Radiative heating rates in subvisible cirrus clouds (optical depth $\tau <$ 0.03) with a thickness of ~500 m in the TTL are ~1–3 K/d [*Jensen et al.*, 1996a; *McFarquhar et al.*, 2000; *Hartmann et al.*, 2001; *Fueglistaler and Fu*, 2006], an order of magnitude smaller than in thick anvil clouds [*Ackerman et al.*, 1988] but an order of magnitude larger than that of air in the TTL. The time mean, tropical mean impact of these thin cirrus clouds on radiative heating rates is about an order of magnitude smaller than that in the cloud (i.e., ~0.2 K/d) [e.g., *Jensen et al.*, 1996a; *Hartmann et al.*, 2001; *Rosenfield et al.*, 1998; *Corti et al.*, 2005]. In the presence of underlying, optically thick clouds, cloud radiative heating rates may also be negative [*Hartmann et al.*, 2001]. However, this occurs relatively infrequently [*Wang and Dessler*, 2006], such that their heating effect probably dominates over the rare cases where cooling occurs [*Fueglistaler and Fu*, 2006]. Generally, clouds in the TTL are found to have a net heating effect, and consequently, they lower the LZRH [*Gettelman et al.*, 2004a; *Corti et al.*, 2005]. Cloud radiative heating effects are currently not well quantified, but it is clear that their net time and area mean impact on radiative heating rates in the TTL is similar to that of clear air and hence have to be accurately represented in models in order to have a realistic heat budget in the TTL (see, e.g., discussion by *Boville et al.* [2006]).

[57] Finally, optically thick clouds in the lower part of the TTL also significantly change radiative fluxes above (with suppressed longwave but enhanced shortwave upward flux). For regions of frequent deep convection, *Fueglistaler and Fu* [2006] calculate for the lower stratosphere ~0.2 K/d lower radiative heating because of the presence of tropospheric clouds, such that in the deep tropics over regions like the tropical western Pacific, the lower stratosphere may be radiatively weakly cooling.

3.2. Stratospheric Brewer-Dobson Circulation

[58] Some of the behavior in the TTL described in section 2 can be understood as a result of the stratospheric Brewer-Dobson circulation. For a cogent explanation of the theoretical underpinnings of the wave driven Brewer-Dobson circulation, see, e.g., *Holton et al.* [1995]. In the zonal mean view, the stratosphere has strong zonal winds associated with the polar vortex, and the residual circulation [e.g., *Dunkerton*, 1978] consists of the net transport of air in the meridional (latitude-altitude) plane after accounting for the influence of wave motions on the Eulerian mean circulation. That such a circulation exists was deduced by *Brewer* [1949] from measurements of stratospheric water vapor at middle latitudes. The stratospheric Brewer-Dobson circulation is also key to the "atmospheric tape recorder" signal (see sections 2.4 and 3.6) as it accounts for both the seasonal cycle of tropical tropopause temperatures and the transport in the stratosphere. A key question is why the temperature cycle, extending from the lower stratosphere down to ~125 hPa (section 2.1), is annual rather than semiannual.

[59] In the tropics, the twice-yearly maximum of solar heating on the equator helps to produce semiannual variations both in the troposphere [e.g., *Weickmann and Chervin*, 1988] and in the upper stratosphere [e.g., *Dunkerton and Delisi*, 1985]. The annual cycle of middle atmosphere mean zonal wind is almost antisymmetric about the equator and therefore has negligible amplitude at the equator [e.g., *Dunkerton and Delisi*, 1985]. Semiannual variations of wind and temperature dominate the upper stratosphere and mesosphere. Much of the seasonal variation in the 20–30 km layer is masked by the QBO of the tropical lower stratosphere [*Baldwin et al.*, 2001]. Nonetheless, the annual cycle of temperature in the lower stratosphere and TTL is remarkably larger than the annual cycle at other tropical altitudes (see Figure 4c).

[60] Early hypotheses for this annual cycle focused on a mechanism tied to the tropical tropospheric circulation [e.g., *Reed and Vlcek*, 1969; *Reid and Gage*, 1981]. A radically different explanation, based on a stratospheric mechanism, was provided by *Yulaeva et al.* [1994]. They showed that there is substantial compensation in the lower stratospheric seasonal temperature variations between the tropics and extratropics, consistent with the idea that the seasonal temperature variation is dynamically driven, and that periods of stronger overturning require stronger diabatic heating/cooling in the ascending/descending branch, which in turn requires lower/higher temperatures. (That is, it is assumed that in the Newtonian cooling approximation (equation (1)) the change in radiative heating is achieved from changing primarily T.) The annual cycle then is a consequence of the fact that the Brewer-Dobson circulation is strongest in boreal winter and weakest during austral winter [see also *Rosenlof*, 1995].

[61] *Randel et al.* [2002] argue that the vertical confinement of maximum temperature amplitude to a layer of less than 10 km (see Figure 4) is related to the long radiative time scale there (see section 3.1). The decrease in amplitude with height in the lower stratosphere may then be linked to a decrease in the radiative time scale. They show that the correspondence of stratospheric wave breaking and tropical temperature response also holds on subseasonal (10–

40 days) time scales. Moreover, there is some evidence that the mechanism also explains interannual variations [*Yulaeva et al.*, 1994; *Randel et al.*, 2006].

[62] Hence, the stratospheric circulation is to be understood as an indirect, eddy-driven circulation. Although the waves probably mainly originate in the extratropical troposphere, they may propagate equatorward, with significant wave breaking also over the subtropics [*Holton et al.*, 1995; *Haynes*, 2005]. Upwelling in the lower stratosphere may be enhanced over the subtropics [*Plumb and Eluszkiewicz*, 1999], and mechanisms driving near-equatorial and cross-equatorial upwelling are under discussion [see, e.g., *Haynes et al.*, 1991; Plumb and Eluskiewicz, 1999; *Plumb*, 2002; *Semeniuk and Shepherd*, 2001; *Scott*, 2002]. The mechanism described here explains much of Figure 4 and implies that an important feature of the TTL is the influence of the Brewer-Dobson circulation that begins already below the tropopause and increases with height in the TTL.

[63] An open question at this point is to what degree also tropical waves may force a residual circulation in the TTL. Using a global primitive equation model driven by observed eddy momentum flux convergence (dominated by equatorial Rossby waves), *Boehm and Lee* [2003] obtained upwelling on the equator peaking at 16.5 km at 0.4 mm/s and sinking below ~14 km. Unlike the Brewer-Dobson circulation, this circulation has a semiannual cycle with maxima in January and July. *Kerr-Munslow and Norton* [2006] pointed out that in the ECMWF 15-year reanalysis (ERA-15) data, a substantial fraction of the wave momentum deposition in the TTL and lower stratosphere appears to arise from quasi-stationary waves in the tropics. On the basis of these findings and model calculations, *Norton* [2006] challenges the explanation proposed by *Yulaeva et al.* [1994] and instead proposes that it is the seasonally varying strength of tropical Rossby waves that drives the annual cycle in upwelling and hence temperatures (with weaker upwelling when the heat source is placed away from the equator, as is the case for the boreal summer). *Randel et al.* [2008] analyze ERA-40 and NCEP/National Center for Atmospheric Research reanalysis data and conclude that the annual cycle in upwelling is forced by subtropical eddy momentum flux convergence due to waves originating both in the tropics and extratropics.

[64] The mechanisms controlling upwelling in the TTL are also tightly coupled to the meridional velocity field. Tracer observations in the lower stratosphere [e.g., *McCormick et al.*, 1993; *Volk et al.*, 1996; *Minschwaner et al.*, 1996; *Randel et al.*, 2001] show rapid meridional mixing and transport out of the tropics (see arrows in Figure 1) up to ~60 hPa; higher up, air masses in the inner tropics experience less (horizontal) mixing than over the middle latitudes (the "surf zone" [*McIntyre and Palmer*, 1984]). This relative isolation of the tropics seen in tracer distributions led to the notion of a "tropical pipe" in the stratosphere [*Plumb*, 1996; see also *Polvani et al.*, 1995]. (See schematics in Figure 1.)

[65] Finally, we note that the time mean stratospheric circulation is generally thought to be fairly zonally uniform. Consequently, its main effect on the TTL is likely that it imposes a seasonally varying zonal mean upwelling, but we must turn to the tropospheric circulation to seek explanations for the observed prominent spatial structures of circulation and temperature as shown in section 2.

3.3. Tropospheric Circulation

[66] The thermodynamically direct Hadley circulation (Figure 3a) consists of rising motion in the tropics, poleward flow in the upper troposphere, sinking in the subtropics, and return flow near the surface [e.g., *Held and Hou*, 1980]. The rising branch migrates seasonally, being generally found in the summer hemisphere, but does not merely follow the latitude of maximum solar heating, owing in part to complexities of ocean dynamics. For example, in the eastern Pacific the rising branch of the Hadley circulation is almost always several degrees latitude north of the equator even in Southern Hemisphere summer.

[67] An analogous circulation occurs along the equatorial belt (longitude-height plane) in the Pacific Ocean (see Figure 6) and is known as the Walker circulation. The rising branch is generally found in the western Pacific over the "maritime continent." Eastward flow typically occurs in the upper troposphere, and the sinking branch of the Walker circulation is typically in the eastern Pacific. Westward flow occurs near the equator. In some respects the Hadley and Walker circulations are similar, with the rising branch in convection and the sinking branch in areas of low precipitation, generally clear skies or only shallow low clouds, and low relative humidity through much of the depth of the troposphere.

[68] The third circulation pattern in the tropics relevant to the TTL is the set of upper tropospheric anticyclones (in the longitude-latitude plane) associated with the Asian and to a lesser extent North American summer monsoons (see Figure 5) in boreal summer and those associated with convection over the maritime continent in boreal winter. The existence of a weak anticyclone in the Southern Hemisphere during boreal summer reveals cross-equatorial coupling of dynamics in the tropical upper troposphere and in the TTL [e.g., *Sardeshmukh and Hoskins*, 1988], and in general, the circulation in the TTL is more symmetric about the equator than in the troposphere. The scale of vertical penetration in linear wave theory is proportional to the horizontal scale, and the anticyclones can be observed up to 70 hPa and higher [*Dunkerton*, 1995].

[69] Both stationary and transient waves are fundamentally important to the structure and variability of the TTL. The structure of the circulation patterns shown in Figures 5 and 6 can be explained in terms of planetary-scale, quasi-stationary Rossby (to the west) and Kelvin (to the east) wave responses to localized heating near the equator [*Matsuno*, 1966; *Gill*, 1980; see also *Jin and Hoskins*, 1995; *Highwood and Hoskins*, 1998; *Randel and Wu*, 2005; *Dima and Wallace*, 2007]. Transient equatorial Kelvin waves have long been observed in the TTL [*Wallace and Kousky*, 1968] and affect tropopause height, temperature, cloud top height [*Shimizu and Tsuda*, 1997], cloud occurrence [*Boehm and*

Verlinde, 2000; *Holton et al.*, 2001], and dehydration [*Jensen and Pfister*, 2004]. Kelvin waves have also been implicated in the transport of dry, ozone-rich air from the stratosphere to the troposphere [*Fujiwara et al.*, 1998, 2001] and in generating turbulence at the tropopause [*Fujiwara et al.*, 2003]. The vertical group velocity of convectively generated gravity waves is rapidly reduced as they travel from the troposphere to the stratosphere owing to the sharp increase in static stability, and temperature soundings often suggest an abrupt increase of wave amplitude above the tropopause, with multiple minima that often make the actual tropopause difficult to locate in individual soundings [e.g., *Selkirk*, 1993; *Reid and Gage*, 1996; *Randel and Wu*, 2005].

[70] On intraseasonal time scales, conditions in the TTL are affected by the eastward propagating Madden-Julian Oscillation (MJO) [*Madden and Julian*, 1971, 1994], which consists of slow moving (5–8 m/s) convective disturbances in the Indian and Pacific oceans and faster (15 m/s) dry disturbances in the eastern Pacific and Atlantic sectors. The MJO has been shown to affect TTL temperatures [*Madden and Julian*, 1994; *Mote et al.*, 2000; *Zhou and Holton*, 2002], water vapor [*Clark et al.*, 1998; *Mote et al.*, 2000; *Eguchi and Shiotani*, 2004] and carbon monoxide [*Wong and Dessler*, 2007], and cirrus clouds [*Eguchi and Shiotani*, 2004]. In the convective portion of the MJO, convection moistens and warms the upper troposphere up to ~200 hPa but cools and dries the layer 150–100 hPa.

[71] Interannual variability arises from changes in the distribution of convection associated with ENSO [e.g., *Gettelman et al.*, 2001]. During El Niño phases, the characteristic temperature pattern at tropopause levels (Figure 5) attenuates, and temperatures are fairly uniform. Consequently, troposphere to stratosphere transport and dehydration in the TTL are more zonally uniform during El Niño than during La Niña [*Fueglistaler and Haynes*, 2005].

[72] Hemispheric asymmetries are smallest during the equinoxes (not shown) and largest during boreal summer. Notably, the moist anomalies during boreal summer over the monsoon regions (see Figure 5, water vapor at 100 hPa in July) seem to reach up to the tropopause [e.g., *Randel et al.*, 2001; see also *Bannister et al.*, 2004; *James et al.*, 2008]. Enhanced mixing ratios of typical tropospheric tracers reveal a strong confinement of air masses within the anticyclone [*Park et al.*, 2008]. Interestingly, the anticyclones associated with the American, India/Southeast Asian, and Australian monsoon are characterized by different combinations of ozone and water vapor anomalies in the TTL (see Figure 5).

[73] One of the striking features of recent studies of transport in, and across, the TTL is its high degree of spatial organization, seen both in analysis data [e.g., *Bonazzola and Haynes*, 2004; *Fueglistaler et al.*, 2004] and in atmospheric general circulation models [e.g., *Hatsushika and Yamazaki*, 2003]. In particular, the region of the western Pacific warm pool with frequent deep convection appears as a dominant source of air entering the TTL [*Fueglistaler et al.*, 2004]. During boreal summer, the Indian/Southeast Asian monsoon region [e.g., *Gettelman et al.*, 2004b; *Randel and Park*, 2006] and Tibetan Plateau [*Gettelman et al.*, 2004b; *Randel and Park*, 2006; *Fu et al.*, 2006] also play an important role. Transport studies also successfully linked anomalous tracer observations in the TTL to, for example, convective events over regions of biomass burning [e.g., *Folkins et al.*, 1997; *Notholt et al.*, 2003]. However, an accurate understanding of vertical transport into the TTL remains a major challenge (see also section 3.4).

[74] Lateral mixing between the tropical upper troposphere and extratropical lower stratosphere is limited (see Figure 1, label c) in the region of the subtropical jets with strong gradients in potential vorticity [e.g., *Haynes and Shuckburgh*, 2000]. Mixing across the jets [e.g., *Tuck et al.*, 2003, 2004] occurs more frequently and effectively in boreal summer of the Northern Hemisphere than in boreal winter or in the Southern Hemisphere in either season. Two kinds of processes contribute to this exchange: (1) advection southward and then westward around the southeast side of the monsoon anticyclones and (2) lateral Rossby wave breaking in adjacent oceanic regions, such as over the mid-Pacific. In the region of the so-called ''westerly ducts'' over the eastern Pacific (see Figure 5), Rossby wave breaking events can transport stratospheric air deep into the tropics [e.g., *Horinouchi et al.*, 2000; *Waugh and Polvani*, 2000; *Waugh and Funatsu*, 2003] and also affect deep convection. The dry intrusions from the lowermost stratosphere are accompanied by elevated ozone concentrations [e.g., *Zachariasse et al.*, 2000] that may lead to a net ozone flux into the TTL [e.g., *Jing et al.*, 2004; *Hitchman et al.*, 2004]. However, the fairly constant N_2O concentrations up to the tropopause (see Figures 11b and 11c) suggest that the air mass flux from these intrusions is small and/or that the intrusions are dominated by air masses that never reached higher levels of the stratosphere (see Figure 1, arrow e). The ability to detect in-mixing of stratospheric air from tracer observations depends also on the difference of tracer concentrations between stratospheric and tropospheric air masses. Profiles of HCl (a tracer with a purely stratospheric source) reveal a similar vertical structure of mixing as those of N_2O but indicate some stratospheric in-mixing already at potential temperature levels of ~360 K [*Marcy et al.*, 2007].

[75] The characteristics of the tropospheric circulation (i.e., the meridionally overturning (Hadley) circulation, the zonally overturning (Walker) circulation, and the strong rotational component associated with the monsoons) are responsible for horizontal and to some extent vertical transport within the TTL and induce the characteristic spatial patterns of temperatures (Figure 5, section 2.1), and because they are evanescent with altitude they provide another marker of tropospheric influence.

3.4. Deep Convection

[76] Convection plays an important role in determining the thermodynamic properties and chemical composition of the TTL. The altitude at which convection detrains is

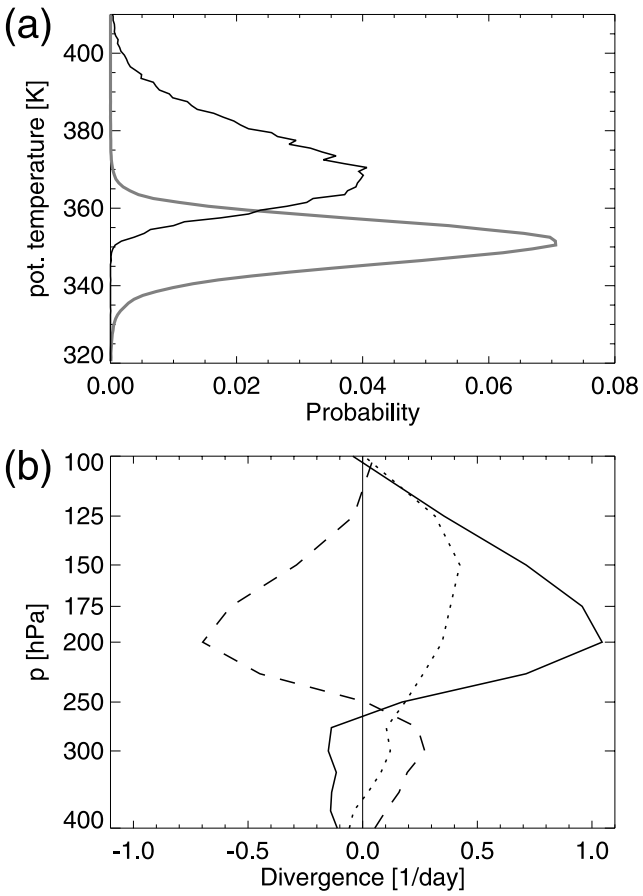

Figure 13. (a) Probability density distribution for cold point potential temperature (black line) and boundary layer equivalent potential temperature (grey line) at Koror, located in the tropical western Pacific. (b) Divergence terms estimated from the Tropical Ocean Global Atmosphere Coupled Ocean Atmosphere Response Experiment (TOGA COARE). Land- and ship-based measurements of horizontal wind between 1 November and 28 February 1993 were used to obtain 6 hourly dynamical divergence profiles. The dynamical divergence profile (δ_d, dotted line) is an average of all 480 divergence profiles stored at the Colorado State University TOGA COARE Sounding Data Archive [*Cieslielski et al.*, 2003]. The convective divergence (solid line) is estimated from the difference of the dynamic (horizontal wind field) divergence (dotted line) and the clear-sky radiative divergence (dashed line).

constrained by the equivalent potential temperature (θ_e, the potential temperature when all latent heat is released) of air parcels near the surface, by convectively available potential energy (CAPE, the vertically integrated buoyancy), and by the degree to which convective updrafts are affected by entrainment (i.e., in-mixing of ambient air masses). On the basis of the theoretical expectation that tropical convection is related to subcloud layer entropy [e.g., *Neelin and Held*, 1987; *Raymond*, 1995], *Folkins and Braun* [2003] find a threshold of $\theta_e \geq 345$ K at which air parcels first attain positive CAPE and may participate in convection. In the absence of mixing, convection will detrain at its level of neutral buoyancy (LNB), which is approximately equal to the height at which its θ_e becomes equal to the potential temperature of the background atmosphere.

[77] Figure 13a (grey line) shows a probability distribution function of pseudoequivalent potential temperature θ_e (which assumes all condensate to be removed immediately) below 900 hPa at Koror (7°N, 134°E). From a purely thermodynamic perspective, most of the air parcels below 900 hPa at Koror exceed the 345 K threshold proposed by *Folkins and Braun* [2003] and are therefore able to participate in deep convection. The distribution of θ_e peaks at ~350 K, and some parcels have θ_e larger than 370 K. The black curve of Figure 13a shows the probability distribution of potential temperature of the cold point tropopause over Koror. The existence of an overlap between the two distributions at Koror shows that some convection in principle could reach the stratosphere locally simply by detrainment at the LNB [see also *Folkins et al.*, 2000]. Also note that a substantial fraction of air parcels has θ_e exceeding the potential temperature of the level of zero net radiative heating (~355 K, see section 3.1). In practice, entrainment of ambient air (with lower θ_e) into the convective updrafts substantially lowers their effective LNB (no simple estimate can be made about how much the LNB is lowered), and other effects such as aerosol loading may also play a role in determining the height of tropical convection.

[78] Air parcels can rise above the LNB by "overshooting" (Figure 1, label h). In general, an air parcel will reach its LNB with a nonzero velocity, having been exposed to an upward buoyancy force below the LNB. The level of maximum overshoot refers to the maximum altitude an air parcel would attain if all the buoyancy work done on the air parcel below the LNB is converted to kinetic energy at the LNB (with velocity proportional to the square root of CAPE), and this kinetic energy is then used to do work against the downward buoyancy force above the LNB. Overshooting air parcels become progressively colder with height than the environment. If they mix with ambient air of higher potential temperature, they will cool these levels and eventually reach equilibrium at an altitude above their initial LNB. *Sherwood* [2000] argued that this cooling would drive descent above vigorous convection, which could explain his finding of net diabatic descent in the stratosphere over the maritime continent. *Sherwood et al.* [2003] further argue that the observed behavior of the cold point over active convective systems requires a role for a direct cooling term due to vertical mixing and propose an area mean cooling in the TTL of order 0.2 K/d, comparable to clear-sky heating rates in the TTL. Some cloud resolving model calculations support this conclusion [*Kuang and Bretherton*, 2004; *Robinson and Sherwood*, 2006], whereas others do not exhibit significant overshooting cooling [*Küpper et al.*, 2004], and results may be sensitive to prescribed boundary conditions.

[79] Although much of tropical convection occurs over the ocean, observations show that convection over land,

possibly related to differences in CAPE (much higher values of CAPE are observed over land [e.g., *Jorgensen and LeMone*, 1989]), tends to produce higher vertical velocities and consequently more overshoot. *Zipser et al.* [2006] show that convective "extreme events" (in terms of height, brightness temperature, and lightning flash rate) predominantly occur over land. However, it is an open question to what extent these (rare) extreme events contribute to transport into the TTL or even into the stratosphere. Also, in the context of the TTL the distinction between individual convective storms and organized mesoscale convective systems [e.g., *Houze*, 1989] may not have received adequate attention in the past. Within hurricanes, the very strong surface winds and low surface pressures have been shown to generate values of near-surface θ_e as large as 370 K [*Schneider and Barnes*, 2005]. *Rossow and Pearl* [2007] (on the basis of ISCCP data) find that most of stratosphere penetrating convection occurs in organized convection.

[80] Direct determination of the detrainment rate profile of convection from observations is difficult, and a number of strategies have been adopted. A diagnostic method to calculate detrainment rate uses wind observations to calculate horizontal ("dynamical") divergence, and radiative transfer calculations to calculate the (diabatic) vertical divergence. Figure 13b illustrates this type of approach following *Folkins et al.* [2006] for the Inner Flux Array of the Tropical Ocean Global Atmosphere Coupled Ocean Atmosphere Response Experiment (TOGA COARE) experiment (diameter $\sim$ 200 km), a region over the western Pacific with intense convection (mean rainfall rate 8.42 mm/d [*Cieslielski et al.*, 2003]). The dashed line shows the diabatic divergence based on clear-sky radiative transfer calculations, and the dotted line shows the dynamical divergence determined from wind observations. Following mass conservation, one can then determine the convective divergence (solid line). We emphasize at this point that the calculation is affected by uncertainties (particularly at upper levels) in the dynamical divergence and radiative transfer calculation, as well as by poorly constrained contributions to the heat budget from advection. Nevertheless, the approach captures the detrainment profile at least qualitatively, with a maximum of convective detrainment around 200 hPa (350 K potential temperature). This maximum coincides with the peak level of θ_e (Figure 13a), and the level of maximum dynamical divergence at 150 hPa coincides with the level of maximum zonal winds of the Walker circulation (Figure 6b). Note that the convective divergence for this particular region (because of its above-average convective activity) is larger than when averaged over the entire tropics.

[81] A survey of published methods to quantify convective mass flux into the TTL shows a variety of methods and metrics, and results agree only qualitatively. Using a similar approach as described above (but assuming that over the entire tropics vertical diabatic mass flux divergence is balanced by detrainment), *Folkins and Martin* [2005] estimate that the convective turnover time is 10 days at 15 km and 60 days at 17 km. On the basis of CO and ozone profiles, *Dessler* [2002] estimated the detrainment rate profile of boundary layer air and obtained a convective turnover time of 20 days at the base of the TTL and $\sim$60 days at the tropopause. The radon measurements of *Kritz et al.* [1993] (see section 2.7.3) yield $\sim$20 days at tropopause levels. On the basis of cloud observations, *Gettelman et al.* [2002b] arrive at a convective turnover time of 4–5 months at the base of the TTL and 1–2 years at the tropopause (with lower values over the western Pacific and Indian Ocean). The time lag of CO_2 concentrations at tropopause levels to those near the surface indicates a transport time scale of $\sim$2 months [*Boering et al.*, 1994; *Strahan et al.*, 1998]. Also on the basis of CO_2 concentrations (but using the slope of the vertical profile), *Park et al.* [2007] report a time lag relative to the boundary layer of $\sim$26 days at 390 K and find observations at 360 K to be indistinguishable from those at the surface.

[82] To summarize, the convective mass flux above the typical level of convective detrainment ($\sim$200 hPa) rapidly decays with height, but there is ample evidence of convective detrainment into the lower parts of the TTL and occasionally even above the tropopause. Because of increasing residence times in the TTL this convective mass flux likely plays an important role in determining its chemical and physical properties. However, large uncertainties in the convective detrainment rate profile remain, and more work on developing a quantitative understanding of the impact of convection is needed.

3.5. Chemistry

[83] In the previous sections we emphasized the importance of various tracers in the TTL and how their abundances are related to atmospheric transport processes. In this section we discuss chemical sources and sinks in the TTL with a focus on species and reactions of relevance for ozone (section 3.5.1) and discuss how processes in the TTL affect stratospheric chemistry (section 3.5.2).

3.5.1. Chemistry in the TTL

[84] In the tropical upper troposphere, ozone chemistry is dominated by the HO_x (being the sum of OH and HO_2, which rapidly convert to each other) and NO_x (being the sum of NO and NO_2, which in turn is a subfamily of total reactive nitrogen, NO_y) cycles. Aircraft measurements from ASHOE/MAESA and STRAT suggest an ozone production rate in the tropical upper troposphere and in the TTL of 1–1.5 ppbv/d [*Wennberg et al.*, 1998; *Folkins et al.*, 2002], though this may be an underestimate due to a sampling bias toward the tropical Pacific. Photolysis of oxygen yields an ozone production of $\sim$0.1 ppbv/d at the bottom of the TTL, increasing to $\sim$2.4 ppbv/d at 400 K [*Dessler*, 2002], such that in the tropical lower stratosphere, the ozone profile can be understood to leading order from photochemical production by oxygen photolysis and upwelling velocity [*Avallone and Prather*, 1996]. In the TTL, however, substantial uncertainties in the rate of ozone production arise from

uncertainties in the geographic distributions (and the chemical budgets) of HO_x and NO_x.

[85] The hydroxyl radical (OH) is the main oxidizing agent in the atmosphere and, as such, affects the rates of production and loss of many species. There have been a number of studies examining the HO_x budget in the tropical upper troposphere, mainly based on measurements of HO_x made during the ASHOE/MAESA and STRAT campaigns [*Jaegle et al.*, 1997; *Folkins et al.*, 1997; *Wennberg et al.,*, 1998]. Measured HO_x mixing ratios were larger than estimated from the known HO_x sinks and HO_x production via the $O(^1D) + H_2O \rightarrow 2OH$ reaction. Because of relatively low H_2O and O_3 mixing ratios, this reaction is less efficient at producing HO_x in the TTL than elsewhere in the troposphere or stratosphere. Other HO_x precursors such as acetone and methyl hydroperoxide could provide the missing HO_x source [*Wennberg et al.*, 1998], though their contribution may be smaller than previously thought [*Arnold et al.*, 2004]. The HO_x budget of the TTL cannot be considered closed also because there have not yet been any simultaneous measurements of HO_x, NO_x, H_2O, CO, and O_3 together with the various postulated HO_x precursors.

[86] The main chemical source of O_3 in the lower part of the TTL is the $NO + HO_2 \rightarrow NO_2 + OH$ reaction, with the reaction of NO with other peroxy radicals probably playing a secondary role. The NO_2 radical produced in these reactions rapidly photolyzes during the day to produce a free oxygen atom ($NO_2 + h\nu \rightarrow NO + O(3P)$), which almost immediately combines with molecular oxygen to produce O_3. Hence, ozone production depends on NO_y, but the budget of NO_y in the TTL is currently not well quantified.

[87] *Ridley et al.* [2004] report from ASHOE/MAESA, STRAT, and Atmospheric Chemistry of Combustion Emissions Near the Tropopause measurements a mean NO/NO_y ratio of $\sim$0.4, which should also be a good estimate of the NO_x/NO_y ratio. (The conversions between NO and NO_2 are dominated by the $NO + O_3$ reaction and the photolysis of NO_2, such that daytime mixing ratios of NO should exceed mixing ratios of NO_2 by at least an order of magnitude.) The NO_x/NO_y ratio will be enhanced by exposure to emissions of NO from lightning or biomass burning and by any irreversible removal of HNO_3 associated with sedimentation of HNO_3-containing particles. Conversely, the NO_x/NO_y ratio will be reduced by processes that increase the rate of oxidation of NO_x to HNO_3, or conversion of NO_x to peroxyacetyl nitrate (PAN). HO_x precursors such as acetone and CH_3OOH would be expected to play a role in reducing the NO_x/NO_y ratio [e.g., *Keim et al.*, 1999], but lack of measurements has precluded a detailed assessment of the factors that govern this ratio.

[88] The remainder of NO_y after subtracting NO_x is probably typically dominated by HNO_3 and PAN. Although there have been some measurements of HNO_3 in the TTL [e.g., *Gao et al.*, 2004], there have been very few measurements of PAN, so that the overall partitioning of NO_y in the TTL is poorly characterized.

[89] The main source for reactive nitrogen in the TTL is probably lightning. Measurements of NO_x at 100 hPa from the HALOE instrument show enhanced NO_x over the continents, presumably arising from convective detrainment of air parcels with lightning-generated NO_x [e.g., *Park et al.*, 2004]. Further, some NO_y could enter the TTL by inmixing of stratospherically older air masses (where some N_2O is converted to NO_y), but the contribution from this source is very uncertain (recall that the profiles shown in Figure 11 show a decrease of N_2O only from the tropopause upward).

[90] The primary loss processes of NO_y from the TTL are probably horizontal export to midlatitudes or upward vertical transport to the stratosphere. However, as with other ice-soluble species, HNO_3 could be irreversibly removed from the TTL via adsorption onto ice particles of sufficient size and fall velocity. *Popp et al.* [2004] report HNO_3 containing ice particles in thin cirrus clouds over the subtropics, and some observations also suggest the existence of nitric acid trihydrate particles in the TTL [*Popp et al.*, 2006].

3.5.2. Impact on Stratospheric Chemistry

[91] Chemical and dynamical processes in the TTL determine the mixing ratios of air parcels entering the stratosphere. Of particular interest are VSL species that contain bromine. VSL substances are defined as those whose atmospheric lifetimes are less than 0.5 year [*Chipperfield et al.*, 2006]. The rate of ozone destruction in the lower stratosphere is very sensitive to the concentration of BrO [*Salawitch et al.*, 2005]. The stratospheric mixing ratio of BrO is believed to be higher than can be accounted for on the basis of the mixing ratios of the known long-lived bromine source gases (primarily halons and CH_3Br) [*Chipperfield et al.*, 2006]. It has therefore been suggested that bromine-containing VSL species may provide the missing bromine source.

[92] The efficiency with which the bromine within a VSL species such as $CHBr_3$ can be delivered to the stratosphere depends on the mean mixing ratio of the source species in air parcels detraining into the TTL, the residence time in the TTL, the photochemical lifetime of the species in the TTL, and the extent to which any ice-soluble bromine released by photochemical degradation of a VSL compound is heterogeneously removed from the TTL by adsorption onto ice crystals of sufficient size and fall velocity. If the photochemical lifetime of a species in the TTL is much longer than the typical transit time across the TTL, the efficiency with which the source gas is delivered to the stratosphere can be assumed to be quite high. However, for VSL substances the photochemical lifetime is comparable with or shorter than the typical age of air parcels in the TTL. In this case, the likelihood of stratospheric entry of an ice-soluble product gas arising from the degradation of a source gas (e.g., HBr), will depend on the manner in which TTL dehydration occurs (see also section 3.6). If dehydration occurs primarily during convection, it seems likely that ice-soluble product gases, produced after detrainment from the

photochemical degradation of a source gas, should reach the stratosphere with an efficiency that approaches 100%. On the other hand, if dehydration occurs primarily during slow ascent through the TTL, then the efficiency with which bromine-containing ice-soluble product gases are irreversibly removed should be much higher [*Sinnhuber and Folkins*, 2006].

[93] More generally, uncertainties in the water vapor budget of the TTL give rise to uncertainties in the removal efficiency of a variety of ice-soluble species in the TTL. If the widespread thin cirrus in the TTL (see section 2.5) generate ice crystals sufficiently large to gravitationally settle out of the TTL, they could also remove other stratospherically relevant trace gases such as HCl, HI, HNO_3, H_2SO_4, and aerosol species. This process would limit the effectiveness with which shorter-lived source gases, e.g., CH_3I and dimethyl sulfide, contribute to the iodine and sulfur budgets of the stratosphere. Conversely, additional measurements of ice-soluble species in the TTL, and associated improvements in the understanding of their budget in the TTL, should lead to improvements in our ability to infer the magnitudes of any heterogeneous removal processes in the TTL and new insights into the TTL water vapor budget.

[94] Finally, we note that stratospheric chemistry is also strongly dependent on the efficiency of dehydration in the TTL (see section 3.6). Stratospheric water vapor concentrations directly affect stratospheric HO_x concentrations [e.g., *Dvortsov and Solomon*, 2001] and play a crucial role for the formation of polar stratospheric clouds that allow heterogeneous chemical reactions (involving chlorine species originating from chlorofluorocarbons) that are responsible for the dramatic ozone losses in the polar, in particular Antarctic, stratospheric vortexes.

3.6. Dehydration

[95] The temperature history of an air parcel is a critical factor in determining its water vapor concentration because of the strong temperature dependence of the vapor pressure. Consequently, dehydration and transport are intrinsically coupled, and information about one of the two may allow conclusions with respect to the other. Since *Brewer*'s [1949] deduction that stratospheric air must have crossed the exceptionally cold tropical tropopause, several tropical measurement campaigns and design of spaceborne remote sensing instruments have been inextricably linked to questions regarding a more detailed view of dehydration and transport across the tropical tropopause.

[96] Historically, the following observations pointed to a need for a refined theory on the control of water vapor concentrations at entry into the stratosphere. First, the driest layer (the "hygropause") in the tropical stratosphere was sometimes observed 1–2 km above the cold point tropopause [e.g., *Kley et al.*, 1979]. *Danielsen* [1982, 1993] suggested that convection penetrating into the stratosphere leads to clouds in the stratosphere with strong radiative cooling, and correspondingly low vapor pressure, at the top of these clouds. Neither numerical models nor observations supported these ideas. *Potter and Holton* [1995] showed in a model study that gravity waves above strong convection may induce cloud formation above the time mean cold point, but the detection of the "atmospheric tape recorder" effect [*Mote et al.*, 1995] (see also section 3.2) largely resolved the issue.

[97] Second, it was argued that the absence of persistent cirrus decks at the tropopause contradicts what one would expect if air were spatially uniformly rising and thus, up to the tropopause, cooling [*Robinson*, 1980]. However, the argument ignores that cloud-free, subsaturated regions may result from horizontal flow on sloping isentropes with corresponding temperature gradients (which are pronounced in the TTL, recall Figures 6a and 5). More recent lidar observations show that clouds at tropopause level are very frequent but optically thin (see section 2.5).

[98] Finally, it was argued that the stratosphere is drier than expected from average tropical tropopause temperatures [*Newell and Gould-Stewart*, 1981]. They drew attention to the fact that the spatial pattern of tropopause temperatures must play a role and suggested that air may enter the stratosphere preferentially at locations and during seasons of lowest temperatures (hence their term "stratospheric fountains"). *Dessler* [1998] showed that Newell and Gould-Stewart's analysis was hampered by the use of 100 hPa temperatures rather than cold point temperatures (which induces a warm/moist bias). *Holton and Gettelman* [2001] point out that it may be horizontal rather than vertical motion that ensures that a large fraction of air entering the stratosphere is exposed to the exceptionally low temperatures observed over the tropical western Pacific/maritime continent area. Using an idealized 2-D model with a realistic temperature distribution in the distance-height plane (with the "distance" axis scaled to match the approximate horizontal distance of the upper level monsoonal anticyclonic motion), they obtained stratospheric water vapor concentrations in reasonable agreement with observations.

[99] Analyses of dehydration based on temperatures without consideration of the circulation are inevitably of very limited value. Consequently, a number of more recent studies took advantage of the improved quality of assimilated temperature and wind fields to study transport and dehydration in the TTL. Despite some limitations regarding the accuracy in particular of vertical transport, trajectory calculations using assimilated data successfully reproduced many observational characteristics. *Gettelman et al.* [2002a] showed that the northward displacement of the first occurrence of the "dry phase" of the tape recorder is a transport phenomenon. Using trajectory calculations based on ERA-40 reanalysis data for the period 1979–2002, *Fueglistaler et al.* [2005] showed that annual mean and seasonal variations of entry mixing ratios, as well as interannual variations [*Fueglistaler and Haynes*, 2005], can be reproduced to within observational uncertainty by the large-scale dynamics and temperatures as resolved by global-scale models.

Interannual variations of entry mixing ratios are dominated by the temperature variations induced by the QBO and ENSO [*Giorgetta and Bengtsson*, 1999; *Scaife et al.*, 2003; *Randel et al.*, 2004; *Fueglistaler and Haynes*, 2005]. Consistent with the hypothesis of large-scale control, *Randel et al.* [2006] link the observed drop of water vapor in 2000/2001 (of 0.2–0.5 ppmv, see section 2.4) to temperature changes at tropopause levels induced by enhanced upwelling (i.e., intensified Brewer-Dobson circulation).

[100] The successful prediction of entry mixing ratios from trajectory calculations based on large-scale winds and temperatures and using a highly simplified cloud scheme may in part be due to a fortuitous cancelation of neglected processes [*Fueglistaler et al.*, 2005]. Using a detailed cloud microphysical model to calculate dehydration during ascent in the TTL, *Jensen and Pfister* [2004] find that the effect of higher-frequency temperature perturbations arising from Kelvin and gravity waves is mostly an increase of cloud particle number densities (with correspondingly smaller crystals), higher cloud occurrence frequency, and changes in geographical distribution but only a weak impact on final water vapor concentrations. Similar conclusions apply to the effects of different nucleation barriers. Recent observations of very high supersaturations both outside [*Jensen et al.*, 2005a] as well as within cirrus clouds [*Jensen et al.*, 2005b] further challenge our understanding of cirrus cloud microphysics and may have an impact on TTL moisture and estimates of entry mixing ratios [*Jensen and Pfister*, 2005]. Apparent supersaturations despite considerable ice surface area density gave rise to speculations whether the ice at these low temperatures may be in cubic (with a higher vapor pressure) rather than hexagonal crystal form [*Murphy*, 2003] or whether HNO_3 on the growing ice crystals may hinder vapor deposition [*Gao et al.*, 2004].

[101] Currently not well quantified is the effect of convection on the TTL water vapor budget. Building on the ideas of *Johnston and Solomon* [1979], *Danielsen* [1982, 1993], and others, *Sherwood and Dessler* [2000] proposed that deep convection overshooting its LNB (see section 3.4) produces very dry air and that this process is crucial for understanding dehydration in the TTL. They used a simple model to show that this process can produce the observed vertical water vapor and ozone distributions, the typical location of stratiform cloud tops below the mean tropopause, while balancing the energy budget. *Sherwood and Dessler* [2003] further showed that their model is capable of reproducing the "tape recorder" and the seasonal cycle of CO_2 in the lower stratosphere. However, convincing evidence from observations for this process is missing. Rather, a number of observations suggest that the injection of large ice masses due to convection actually leads to a net moistening [e.g., *Corti et al.*, 2008].

[102] Simulations of convection using cloud resolving models yield contradictory results. While *Kuang and Bretherton* [2004] find evidence for convective overshoot to induce drying, *Küpper et al.* [2004] and *Smith et al.* [2006] do not. *Jensen et al.* [2007] find that convection tends to hydrate the TTL unless it is initially supersaturated. *Grosvenor et al.* [2007] find that results from 3-D cloud resolving models yield a moistening effect, whereas 2-D models that cannot resolve realistic wind shear yield a drying effect due to lack of mixing of the overshoot with ambient air.

[103] Further evidence for a role of convection comes from water isotopologue measurements (see section 2.6). *Moyer et al.* [1996] suggested that the observed underdepletion of stratospheric water vapor may be a consequence of the evaporation of isotopically heavy, convectively lofted ice. *Smith et al.* [2006] use a cloud resolving model with isotope physics and find isotopic enrichment in the upper troposphere due to convection but obtained an unrealistic profile of δD across the tropopause. *Dessler et al.* [2007] obtained a more realistic δD profile using trajectories subject to stochastic moistening to mimic the effect of convection. Other modeling studies employ different mechanisms [e.g., *Johnson et al.*, 2001; *Dessler and Sherwood*, 2003; *Gettelman and Webster*, 2005] to arrive at results broadly in agreement with observations. Clearly, more measurements and modeling studies are needed in order to constrain the TTL water budget from water isotopologues.

[104] Interest in dehydration in the TTL also arises from the possibility of a large long-term trend of stratospheric water vapor. *Rosenlof et al.* [2001] reported a multidecadal increase of stratospheric water vapor since the early 1950s of ~1%/a. Only very few observations before the 1980s are available, and trends of the two most important time series, the Boulder Frostpoint Hygrometer measurements and HALOE, show significant differences [*Randel et al.*, 2004]. In a recent reevaluation of the Boulder data, *Scherer et al.* [2008] find a linear trend that is up to 40% smaller than in the original analysis by *Oltmans et al.* [2000], but differences to HALOE remain. Uncertainties in the measurements thus render the magnitude of the water vapor trend uncertain. However, even a small increase that could not be attributed to methane oxidation would pose a major conundrum. *Zhou et al.* [2001] emphasize that from the long-term trend of tropopause temperatures, provided this trend is reliable, one would expect a decrease rather than increase in water vapor entry concentrations. The discrepancy between water and temperature trend cannot be resolved by changes in circulation [*Fueglistaler and Haynes*, 2005], and it may be that changes in cloud microphysical processes play a role. *Sherwood* [2002] suggested that changes in biomass burning may affect cloud particle sizes (and hence dehydration) of deep convective clouds, and *Notholt et al.* [2005] argued that particle sizes of thin cirrus at the tropopause may be affected by increasing SO_2 emissions at low latitudes. However, a recent analysis of stratospheric HDO for the period 1991–2007 did not find indications for a change in the amount of water that entered the stratosphere as particles (Notholt et al., submitted manuscript, 2009).

[105] To summarize, models can reproduce mean entry water vapor concentrations and variations on seasonal and interannual time scales reasonably well but cannot reproduce a positive long-term trend as proposed by *Rosenlof et al.* [2001]. Water isotopologue data may provide additional constraints that will help to further improve our understanding of dehydration in the TTL. A major impediment for rigorous assessment of models remains the unresolved discrepancies between water vapor measurements of different sensors [*Kley et al.*, 2000] and uncertainties of temperature trends in the TTL.

3.7. Entrainment Layer or Eddy-Driven Circulation?

[106] The previous sections have shown how processes both on large (planetary) and small (mesoscale) scales contribute to the unique properties of the TTL. Despite much progress in recent years toward a more unified view, differences still exist in the perception of which processes are instrumental for the TTL as observed. The answer to this question depends on which aspects of the TTL are considered and may be very different for, e.g., the heat budget, the air mass budget, or the budget of a particular tracer. Nevertheless, much of the ongoing discussion revolves around the question whether the key process responsible for the TTL as observed is an eddy-driven (residual) circulation or deep convection. Though they are very different processes, their impact on observable quantities is often surprisingly ambiguous.

[107] It was recognized early that very deep convection has a significant impact on temperatures in the vicinity of the tropopause. Observations showed a direct cooling above convective cells of several kelvins [e.g., *Arakawa*, 1950; *Johnson and Kriete*, 1982], and a number of hypotheses were proposed to explain this behavior. One hypothesis is that turbulent mixing of convective overshoot leads to an irreversible cooling in the mixing layer [e.g., *Sherwood*, 2000]. Other hypotheses (e.g., radiative effects) have not found support. The interpretation of this temperature response, however, is ambiguous as it may be also simply a hydrostatic adjustment to underlying warming without mixing of air parcels [see, e.g., *Holloway and Neelin*, 2007]. In a series of papers, *Danielsen* [1982, 1993] proposed that convection penetrating into the stratosphere plays a major role for troposphere-stratosphere transport and for dehydration. *Sherwood and Dessler* [2003] argue that the characteristics of the water vapor and carbon dioxide seasonal cycles in the TTL and lower stratosphere can be explained by deep overshooting convection, challenging the earlier argument by *Boering et al.* [1995] that their phase coherence suggests only a minor role for deep overshooting convection. Finally, on seasonal time scales, attempts were made to link the annual cycle of temperatures to variations in the Hadley cell circulation [e.g., *Reed and Vlcek*, 1969; *Reid and Gage*, 1981].

[108] In contrast, the paradigm of eddy-driven circulation emerged when the annual cycle of tropical tropopause temperatures was successfully linked to the stratospheric Brewer-Dobson circulation [*Yulaeva et al.*, 1994], and previously troubling observations of the level of the "hygropause" could be explained by the "atmospheric tape recorder" effect [*Mote et al.*, 1996]. From the perspective of an eddy-driven circulation, the zonal mean temperature profile already below the tropopause is strongly affected by the stratospheric Brewer-Dobson circulation. In fact, one may postulate that the (zonal mean circulation of the) TTL already is part of the eddy-driven stratospheric circulation, as evident, e.g., in the annual temperature cycle that extends down to ~125 hPa (360 K, 15.5 km). Some questions remain about the forced upwelling in the tropics, e.g., flow across angular momentum contours [*Plumb and Eluszkiewicz*, 1999] and the role of the quasi-stationary tropical waves. The spatial pattern of temperature in the TTL on monthly time scales results from the quasi-stationary, upper level wave response to heating in convection below [*Gill*, 1980]. The observed eastward tilt of low temperature anomaly over the Pacific is consistent with a Kelvin wave, and the westward extensions are consistent with quasi-stationary Rossby waves. On subseasonal time scales, *Zhou and Holton* [2002] find that temperature anomalies over the Pacific precede enhanced convection (variations due to MJO), also consistent with eastward traveling Kelvin waves.

[109] Another feature of interest is that the tropical tropopause is situated several kilometers above the main convective outflow layer, and understanding the level of the tropopause (not just the tropical) remains an active topic of research [e.g., *Manabe and Strickler*, 1964; *Held*, 1982; *Atticks and Robinson*, 1983; *Frederick and Douglass*, 1983; *Highwood and Hoskins*, 1998; *Thuburn and Craig*, 2000]. *Thuburn and Craig* [2002] show that the aforementioned separation is mainly a radiative phenomenon and exists also in a model without convective overshoot and with a dynamically passive stratosphere. In their model, imposing a net upwelling to mimic the stratospheric residual circulation leads to a lifting of the cold point but not to substantial changes in the vertical temperature structure. Conversely, the model simulations of *Kuang and Bretherton* [2004] produce a tropopause height that is closely tied to convection.

[110] Common to both perspectives is that temperatures in the TTL (in particular also the tropopause) are lower than if it were in radiative equilibrium. The existence of a level of zero net radiative heating arises in both perspectives but for different reasons. From the perspective of convective overshoot, the TTL fundamentally is an entrainment layer, where turbulent (vertical) mixing cools the TTL, which in turn has to be balanced by radiative heating. From the perspective of an eddy-driven circulation, the radiative heating acts to balance the diabatic vertical velocity required by the residual circulation. (Note that even in the absence of an eddy-driven circulation, a net residual circulation might exist because of the latitudinal gradient of absorbed radiation, although this circulation would be much weaker than the real stratospheric circulation.)

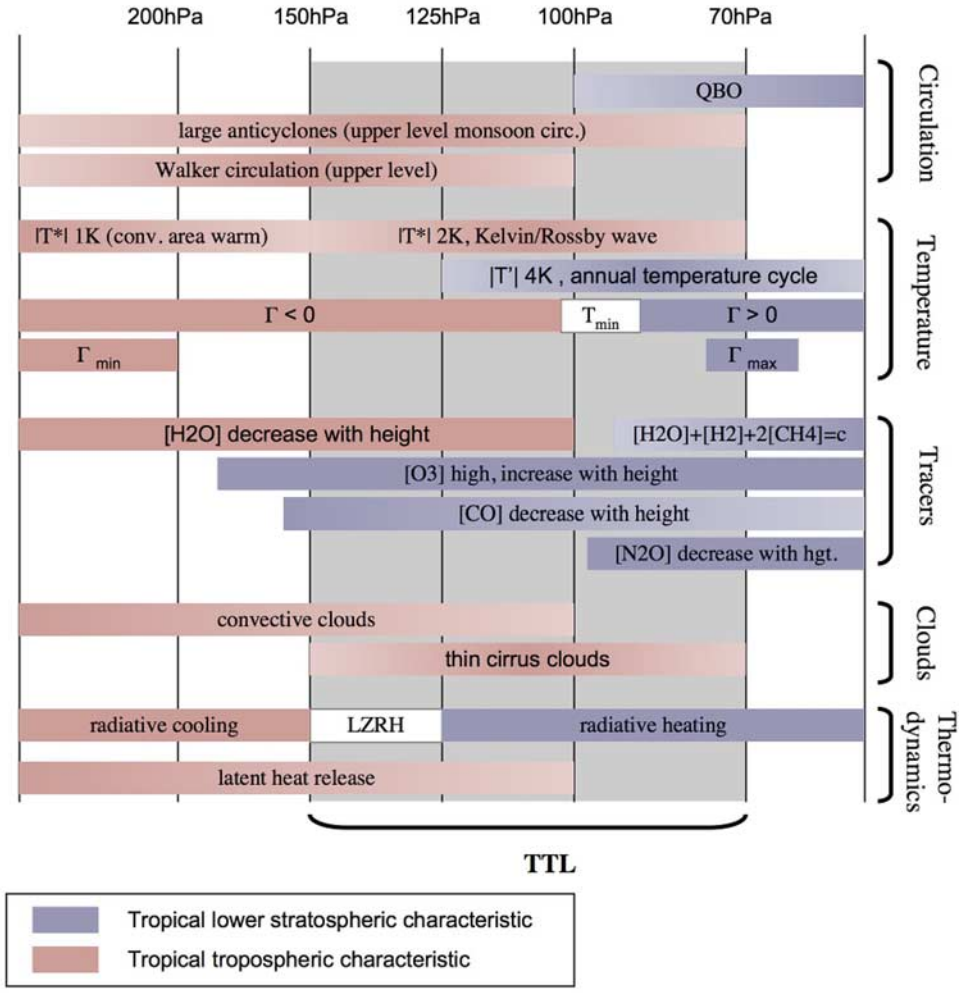

Figure 14. Summary of tropospheric/stratospheric characteristics and transitions thereof (symbolically shown as fade out of colored pattern). Γ, temperature lapse rate; T_{min}, temperature minimum of profile; $|T^*|$, amplitude of quasi-stationary zonal temperature anomaly; $|T'|$, amplitude of tropical mean temperature seasonal cycle; QBO, quasi-biennial oscillation.

[111] From a large-scale point of view, the evidence is in favor of a dominant role of eddy-driven circulations for the spatiotemporal structure of the TTL. However, it is of central importance to quantify to what extent deep convection modifies the properties, in particular also the chemical composition, of the TTL. The question is not merely of academic interest: our ability to predict the state of the stratosphere (specifically, the recovery of the ozone layer) in the coming decades hinges to a good degree on accurate predictions of changes in tropical troposphere to stratosphere transport. The two processes are of quite different nature and consequently may respond very differently to changes in climate forcings.

4. A SYNTHESIS DEFINITION OF THE TTL

[112] Temperature, winds, and tracer distributions presented here show that in the tropics the transition from troposphere to stratosphere occurs over a transition layer rather than at a sharp boundary. Because it is a "transition zone," any definition of boundaries for this layer bears a certain arbitrariness, and currently existing definitions of the TTL disagree about bottom and top bounds and do not address its meridional extent.

[113] Figure 14 summarizes significant levels (on the basis of observations shown in section 2 and theoretical considerations in section 3) in the tropical upper troposphere and lower stratosphere. Our definition of the TTL emphasizes levels associated with temperature and the circulation. Levels observed in chemical tracers often reflect the former but also frequently depend on the particulars of the species considered, such that the information provided by the abundance of a given tracer is not sufficiently generic to define the TTL.

[114] We set the bottom of the TTL at 150 hPa, where temperature anomalies both on short time scales (associated with convection) and on large spatial scales have a local minimum and change sign: warm/cold anomalies below are

TABLE A1. Summary of Data Sources[a]

Source	Data	Figures	Reference/Web Site
ACE-FTS	CO	11	*Bernath et al.* [2005]
ATMOS	HDO, H_2O	10	*Gunson et al.* [1996], data adapted from *Kuang et al.* [2003]
CALIPSO	particles	9	*Winker et al.* [2007], http://www-calipso.larc.nasa.gov/products
ERA-40	wind, T, geopotential	1, 3–6	*Uppala et al.* [2005], http://data.ecmwf.int/data/
HAGAR	N_2O	11	data courtesy C. M. Volk
HALOE	H_2O (v19)	8	*Russell et al.* [1993], http://haloe.gats-inc.com/home/index.php
Harvard Lyman Alpha	H_2O	8	*Weinstock et al.* [1995], http://espoarchive.nasa.gov
ICOS	HDO, H_2O	10	data courtesy T. Hanisco
MLS/UARS	H_2O (v7.02)	8	*Read et al.* [2004], http://mls.jpl.nasa.gov/uars/data.php
MLS/Aura	H_2O, O_3 (v2.2)	5	*Froidevaux et al.* [2006], *Read et al.* [2007], http://mls.jpl.nasa.gov/index-eos-mls.php
SAGE II	extinction	9	data updated and adapted from *Wang et al.* [1996] by P. H. Wang, http://eosweb.larc.nasa.gov/PRODOCS/sage2/table_sage2.html
SHADOZ	O_3, T	2, 7	*Thompson et al.* [2003a], http://croc.gsfc.nasa.gov/shadoz/
TOGA COARE	wind, T	13	*Cieslielski et al.* [2003], http://www.ncdc.noaa.gov/oa/coare

[a]ACE-FTS, Atmospheric Chemistry Experiment–Fourier Transform Spectrometer; ERA-40, European Centre for Medium Range Weather Forecasts 40-year reanalysis; SHADOZ, Southern Hemisphere Additional Ozonesondes. For other acronyms, see Tables A2 and A3.

associated with cold/warm anomalies above. On seasonal time scales, temperatures above this level begin to show the annual cycle typical for the lower stratosphere. The vertical temperature profile shows a lapse rate minimum in a broad layer below but begins to substantially increase around 150 hPa. This level is also about where the (all-sky) LZRH is observed. Below, the dominant terms of the heat budget are radiative cooling and latent heat release within the tropics (with excess heat exported to higher latitudes), whereas above that level, radiative heating over the low latitudes is balanced by radiative cooling over the high latitudes. These observations show that from ~150 hPa upward, the direct impact of convection (heating due to latent heat release) loses its dominant influence on the thermal structure.

[115] The definition of the top at 70 hPa emphasizes that the horizontal circulation patterns (e.g., upper level monsoonal anticyclones) up to that level are strongly influenced by tropical tropospheric processes, i.e., the geographical distribution of (convective) heating. Also, temperature shows coherent quasi-stationary geographical structure in the layer 150–70 hPa. Whether coincidentally or not, 70 hPa is also about the level of maximum static stability and is the highest levels where clouds (and hence modifications in the water budget) occasionally may be still observed.

[116] It appears that in particular in the upper part of the TTL, lateral tracer transport is less suppressed than either below or above. It is thus difficult to locate lateral boundaries, and we propose mainly for practical reasons the latitude belt on the equatorward side of the subtropical jets (i.e., at latitudes lower than ~30°).

[117] The definition of the TTL as proposed here differs from some previously published definitions. In particular, *Gettelman and de Forster* [2002] set the lower bounds of the TTL at the level of potential temperature lapse rate minimum (which they located between 10 and 12 km) and the top at the (cold point) tropopause. We regard the former as being a typical feature of the troposphere. Consequently, we consider the potential temperature lapse rate minimum as being too low for being the lower boundary of a layer with both tropospheric and stratospheric characteristics. Conversely, it appears to us that the traditional tropopause levels (in the classical sense of either the World Meteorological Organization definition or cold point) exhibit in many ways "maximum TTL characteristics" and hence should be part of the TTL, rather than its upper bound.

5. OUTLOOK

[118] Our understanding of the processes active in the TTL has greatly improved in recent years. Much progress has been made regarding the processes that control stratospheric water vapor, but we note that the observation of supersaturation within clouds could indicate interesting peculiarities of cloud microphysics in the TTL, perhaps associated with the very low temperatures in that layer. Observed increases in stratospheric water vapor, though perhaps smaller than originally published, still cannot be fully reconciled with current model calculations. Predicting changes in the TTL due to increasing greenhouse gas concentrations remains a challenge. Current data of multidecadal temperature trends (hampered by uncertainties and biases in observations) suggest a slight cooling of the TTL (at 100 hPa, −0.15 to −0.35 K/decade for 1959–1997 and −0.6 to −0.8 K/decade for 1979–1997 [*Lanzante et al.*, 2003]), with a transition from warming to cooling just below the TTL (at 150 hPa for 1959–1997 and at ~250 hPa

TABLE A2. Acronyms of Instruments and Platforms

Acronym	Definition
ATMOS	Atmospheric Trace Molecule Spectroscopy experiment
CALIPSO	Cloud-Aerosol Lidar and Infrared Pathfinder Satellite Observation
HALOE	Halogen Occultation Experiment
HAGAR	High Altitude Gas Analyser
ICOS	Integrated Cavity Output Spectroscopy
MLS	Microwave Limb Sounder
SAGE II	Stratospheric Aerosol and Gas Experiment
UARS	Upper Atmosphere Research Satellite

TABLE A3. Acronyms of Measurement Campaigns[a]

Acronym	Definition
ACCENT	Atmospheric Chemistry of Combustion Emissions Near the Tropopause (1999–2000)
APE-THESEO	Airborne Platform for Earth observation–Third European Stratospheric Experiment on Ozone (1999)
ASHOE/MAESA	Airborne Southern Hemisphere Ozone Experiment/Measurements for Assessing the Effects of Stratospheric Aircraft (1994)
CEPEX	Central Equatorial Pacific Experiment (1993)
PRE-AVE	Pre–Aura Validation Experiment (2004)
TROCCINOX	Tropical Convection, Cirrus and Nitrogen Oxides experiment
SCOUT-Tropical	Stratospheric-Climate links with emphasis on the upper Troposphere and lower stratosphere, deployment in Darwin, Australia (2005)
SCOUT/AMMA	Stratospheric-Climate links with emphasis on the upper Troposphere and lower stratosphere, deployment in Africa jointly with African Monsoon Multidisciplinary Analyses project (2006)
STEP	Stratosphere-Troposphere Exchange Project (1987)
STRAT	Stratospheric Tracers of Atmospheric Transport (1995–1996)
TOGA COARE	Tropical Ocean Global Atmosphere Coupled Ocean Atmosphere Response Experiment

[a]Alphabetically, with date.

for 1979–1997 [*Lanzante et al.*, 2003]), but it is not clear which processes are accountable for these changes. Perhaps most importantly, the convective detrainment rate profile is still poorly quantified, and the effect of overshooting convection on the heat balance of the TTL is still a major unknown. Both of these play an important role also for transport time scales into the stratosphere. There is currently also some debate regarding the processes driving upwelling in the TTL, and it is hoped that this issue will be resolved soon. Understanding all processes that control the TTL, and incorporating them in models, is an important prerequisite for reliable predictions of changes in the TTL in a changing climate and for predicting how these changes in turn feed back, e.g., via stratospheric ozone chemistry, on the global climate system.

APPENDIX A

[119] A complete list of data sources for each figure of this paper is provided in Table A1. Acronyms for instruments and platforms and for measurement campaigns are provided in Tables A2 and A3.

[120] **ACKNOWLEDGMENTS.** We would like to thank numerous colleagues who have helped in many ways in the preparation of this review. We received helpful comments and suggestions on an early version of this manuscript from A. Gettelman, E. Jensen, W. J. Randel, and S. Sherwood. We are grateful to T. Hanisco and C. M. Volk who kindly provided data prior to publication and to P.-H. Wang for providing data particularly for this paper. Z. Kuang and A. Gettelman kindly provided previously published data. Finally, we thank three anonymous reviewers for their helpful comments and suggestions.

[121] The Editor responsible for this paper was Gerald North. He thanks two anonymous technical reviewers.

REFERENCES

Ackerman, T. P., K. N. Liou, F. P. J. Valero, and L. Pfister (1988), Heating rates in tropical anvils, *J. Atmos. Sci.*, *45*, 1606–1623.

Arakawa, H. (1950), Analysis of the tropopause and the stratospheric field of temperature of a mature typhoon, *Pap. Meteorol. Geophys.*, *2*, 1–5.

Arnold, S. R., M. P. Chipperfield, M. A. Blitz, D. E. Heard, and M. J. Pillling (2004), Photodissociation of acetone: Atmospheric implications of temperature-dependent quantum yields, *Geophys. Res. Lett.*, *31*, L07110, doi:10.1029/2003GL019099.

Atticks, M. G., and G. D. Robinson (1983), Some features of the structure of the tropical tropopause, *Q. J. R. Meteorol. Soc.*, *109*, 295–308.

Avallone, L. M., and M. J. Prather (1996), Photochemical evolution of ozone in the lower tropical stratosphere, *J. Geophys. Res.*, *101*(D1), 1457–1461.

Baldwin, M. P., et al. (2001), The quasi-biennial oscillation, *Rev. Geophys.*, *39*(2), 179–229.

Bannister, R. N., A. O'Neill, A. R. Gregory, and K. M. Nissen (2004), The role of the south-east Asian monsoon and other seasonal features in creating the 'tape-recorder' signal in the Unified Model, *Q. J. R. Meteorol. Soc.*, *130*, 1531–1554.

Bernath, P. F., et al. (2005), Atmospheric Chemistry Experiment (ACE): Mission overview, *Geophys. Res. Lett.*, *32*, L15S01, doi:10.1029/2005GL022386.

Boehm, M. T., and S. Lee (2003), The implications of tropical Rossby waves for tropical tropopause cirrus formation and for the equatorial upwelling of the Brewer-Dobson circulation, *J. Atmos. Sci.*, *60*, 247–261.

Boehm, M. T., and J. Verlinde (2000), Stratospheric influence on upper tropospheric tropical cirrus, *Geophys. Res. Lett.*, *27*, 3209–3212.

Boering, K. A., S. C. Wofsy, M. Loewenstein, J. R. Podolske, and E. R. Keim (1994), Tracer-tracer relationships and lower stratospheric dynamics: CO_2 and N_2O correlations during SPADE, *Geophys. Res. Lett.*, *21*(23), 2567–2570, doi:10.1029/94GL01985.

Boering, K. A., et al. (1995), Measurements of stratospheric carbon dioxide and water vapor at northern midlatitudes: Implications for troposphere-to-stratosphere transport, *Geophys. Res. Lett.*, *22*(20), 2737–2740.

Bonazzola, M., and P. H. Haynes (2004), A trajectory-based study of the tropical tropopause region, *J. Geophys. Res.*, *109*, D20112, doi:10.1029/2003JD004356.

Boville, B. A., P. J. Rasch, J. J. Hack, and J. R. McCaa (2006), Representation of clouds and precipitation processes in the Community Atmosphere Model Version 3 (CAM3), *J. Clim.*, *19*, 2184–2198.

Bresser, G., A. J. L. Manning, S. Pawson, and C. D. Rodgers (1995), A new parameterization of scale-dependent radiative rates in the stratosphere, *J. Atmos. Sci.*, *52*, 4429–4447.

Brewer, A. W. (1949), Evidence for a world circulation provided by the measurements of helium and water vapor distribution in the stratosphere, *Q. J. R. Meteorol. Soc.*, *75*, 351–363.

Chipperfield, M. P., et al. (2006), Global ozone: Past and present, in *Scientific Assessment of Ozone Depletion: 2006, Global Ozone Res. and Monit. Proj., Rep. 50*, pp. 3.1–3.57, World Meteorol. Organ., Geneva, Switzerland.

Cieslielski, P. E., R. H. Johnson, P. T. Haerrel, and J. Wang (2003), Corrected TOGA COARE sounding humidity data: Impact on diagnosed properties of convection and climate over the warm pool, *J. Clim.*, *16*, 2370–2384.

Clark, H. L., R. S. Harwood, P. W. Mote, and W. G. Read (1998), Variability of water vapor in the tropical upper troposphere as measured by the Microwave Limb Sounder on UARS, *J. Geophys. Res.*, *103*, 31,695–31,707.

Corti, T., B. P. Luo, T. Peter, H. Vömel, and Q. Fu (2005), Mean radiative energy balance and vertical mass fluxes in the equatorial upper troposphere and lower stratosphere, *Geophys. Res. Lett.*, *32*, L06802, doi:10.1029/2004GL021889.

Corti, T., et al. (2008), Unprecedented evidence for deep convection hydrating the tropical stratosphere, *Geophys. Res. Lett.*, *35*, L10810, doi:10.1029/2008GL033641.

Crutzen, P. J. (1974), Photochemical reactions initiated by and influencing ozone in unpolluted tropospheric air, *Tellus*, *26*(1–2), 47–57.

Danielsen, E. F. (1982), A dehydration mechanism for the stratosphere, *Geophys. Res. Lett.*, *9*, 605–608.

Danielsen, E. F. (1993), In situ evidence of rapid, vertical, irreversible transport of lower tropospheric air into the lower tropical stratosphere by convective cloud turrets and by larger-scale upwelling in tropical cyclones, *J. Geophys. Res.*, *98*, 8665–8681.

Dessler, A. E. (1998), A reexamination of the 'stratospheric fountain' hypothesis, *Geophys. Res. Lett.*, *25*(22), 4165–4168.

Dessler, A. E. (2002), The effect of deep, tropical convection on the tropical tropopause layer, *J. Geophys. Res.*, *107*(D3), 4033, doi:10.1029/2001JD000511.

Dessler, A. E., and H. Kim (1999), Determination of the amount of water vapor entering the stratosphere based on Halogen Occultation Experiment (HALOE) data, *J. Geophys. Res.*, *104*, 30,605–30,607.

Dessler, A. E., and S. C. Sherwood (2003), A model of HDO in the tropical tropopause layer, *Atmos. Chem. Phys.*, *3*, 2173–2181.

Dessler, A. E., and P. Yang (2003), The distribution of tropical thin cirrus clouds inferred from Terra MODIS data, *J. Clim.*, *16*, 1241–1247.

Dessler, A. E., S. P. Palm, and J. D. Spinhirne (2006), Tropical cloud-top height distributions revealed by the Ice, Cloud, and Land Elevation Satellite (ICESat)/Geoscience Laser Altimeter System (GLAS), *J. Geophys. Res.*, *111*, D12215, doi:10.1029/2005JD006705.

Dessler, A. E., T. F. Hanisco, and S. Fueglistaler (2007), The effects of convective ice lofting on H_2O and HDO in the TTL, *J. Geophys. Res.*, *112*, D18309, doi:10.1029/2007JD008609.

Dima, I., and J. M. Wallace (2007), Structure of the annual-mean equatorial planetary waves in the ERA-40 reanalyses, *J. Atmos. Sci.*, *64*, 2862–2880, doi:10.1175/JAS3985.1.

Dunkerton, T. (1978), On the mean meridional mass motions of the stratosphere and mesosphere, *J. Atmos. Sci.*, *35*, 2325–2333.

Dunkerton, T. J. (1995), Evidence of meridional motion in the summer lower stratosphere adjacent to monsoon regions, *J. Geophys. Res.*, *100*(D8), 16,675–16,688.

Dunkerton, T. J., and D. P. Delisi (1985), Climatology of the equatorial lower stratosphere, *J. Atmos. Sci.*, *42*(4), 376–396.

Dvortsov, V. L., and S. Solomon (2001), Response of the stratospheric temperatures and ozone to past and future increases in stratospheric humidity, *J. Geophys. Res.*, *106*(D7), 7505–7514.

Eguchi, N., and M. Shiotani (2004), Intraseasonal variations of water vapor and cirrus clouds in the tropical upper troposphere, *J. Geophys. Res.*, *109*, D12106, doi:10.1029/2003JD004314.

Engel, A., C. Schiller, U. Schmidt, R. Borchers, H. Ovarlez, and J. Ovarlez (1996), The total hydrogen budget in the Arctic winter stratosphere during the European Arctic Stratospheric Ozone Experiment, *J. Geophys. Res.*, *101*, 14,495–14,504.

Fels, S. B. (1982), A parameterization of scale-dependent radiative damping rates in the middle atmosphere, *J. Atmos. Sci.*, *39*, 1141–1152.

Filipiak, M. J., R. S. Harwood, J. H. Jiang, Q. Li, N. J. Livesey, G. L. Manney, W. G. Read, M. J. Schwartz, J. W. Waters, and D. L. Wu (2005), Carbon monoxide measured by the EOS Microwave Limb Sounder on Aura: First results, *Geophys. Res. Lett.*, *32*, L14825, doi:10.1029/2005GL022765.

Fishman, J., C. E. Watson, J. C. Larsen, and J. A. Logan (1990), Distribution of tropospheric ozone determined from satellite data, *J. Geophys. Res.*, *95*, 3599–3617.

Folkins, I. (2002), Origin of lapse rate changes in the upper tropical troposphere, *J. Atmos. Sci.*, *59*, 992–1005.

Folkins, I., and C. Braun (2003), Tropical rainfall and boundary layer moist entropy, *J. Clim.*, *16*(11), 1807–1820.

Folkins, I., and R. V. Martin (2005), The vertical structure of tropical convection and its impact on the budgets of water vapor and ozone, *J. Atmos. Sci.*, *62*, 1560–1573.

Folkins, I., R. Chatfield, D. Baumgardner, and M. Proffit (1997), Biomass burning and deep convection in southeastern Asia: Results from ASHOE/MAESA, *J. Geophys. Res.*, *102*(D11), 13,291–13,299.

Folkins, I., M. Loewenstein, J. Podolske, S. J. Oltmans, and M. Proffit (1999), A barrier to vertical mixing at 14 km in the tropics: Evidence from ozoneondes and aircraft measurements, *J. Geophys. Res.*, *104*(D18), 22,095–22,102.

Folkins, I., S. J. Oltmans, and A. M. Thompson (2000), Tropical convective outflow and near surface equivalent potential temperatures, *Geophys. Res. Lett.*, *27*(16), 2549–2552.

Folkins, I., C. Braun, A. M. Thompson, and J. Witte (2002), Tropical ozone as an indicator of deep convection, *J. Geophys. Res.*, *107*(D13), 4184, doi:10.1029/2001JD001178.

Folkins, I., P. Bernath, C. Boone, G. Lesins, N. Livesay, A. M. Thompson, K. Walker, and J. Witte (2006), Seasonal cycles of O_3, CO, and convective outflow at the tropical tropopause, *Geophys. Res. Lett.*, *33*, L16802, doi:10.1029/2006GL026602.

Forster, P. M. de F., and K. P. Shine (1999), Stratospheric water vapour changes as a possible contributor to observed stratospheric cooling, *Geophys. Res. Lett.*, *26*(21), 3309–3312.

Frederick, J. E., and A. R. Douglass (1983), Atmospheric temperatures near the tropical tropopause: Temporal variations, zonal asymmetry and implications for stratospheric water vapor, *Mon. Weather Rev.*, *11*, 1397–1403.

Froidevaux, L., et al. (2006), Early validation analyses of atmospheric profiles from EOS MLS on the Aura satellite, *IEEE Trans. Geosci. Remote Sens.*, *44*(5), 1106–1121.

Fu, Q., and K. N. Liou (1992), On the correlated k-distribution method for radiative transfer in nonhomogeneous atmospheres, *J. Amos. Sci.*, *49*(22), 2139–2156.

Fu, Q., Y. X. Hu, and Q. Yang (2007), Identifying the top of the tropical tropopause layer from vertical mass flux analysis and CALIPSO lidar cloud observations, *Geophys. Res. Lett.*, *34*, L14813, doi:10.1029/2007GL030099.

Fu, R., Y. Hu, J. S. Wright, J. H. Jiang, R. E. Dickinson, M. Chen, M. Fillipiak, W. G. Read, J. W. Waters, and D. L. Wu (2006), Short circuit of water vapor and polluted air to the global stratosphere by convective transport over the Tibetan Plateau, *Proc. Natl. Acad. Sci. U. S. A.*, *103*(15), 5664–5669.

Fueglistaler, S., and Q. Fu (2006), Impact of clouds on radiative heating rates in the tropical lower stratosphere, *J. Geophys. Res.*, *111*, D23202, doi:10.1029/2006JD007273.

Fueglistaler, S., and P. H. Haynes (2005), Control of interannual and longer-term variability of stratospheric water vapor, *J. Geophys. Res.*, *110*, D24108, doi:10.1029/2005JD006019.

Fueglistaler, S., H. Wernli, and T. Peter (2004), Tropical troposphere-to-stratosphere transport inferred from trajectory calculations, *J. Geophys. Res.*, *109*, D03108, doi:10.1029/2003JD004069.

Fueglistaler, S., M. Bonazzola, P. H. Haynes, and T. Peter (2005), Stratospheric water vapor predicted from the Lagrangian temperature history of air entering the stratosphere in the tropics, *J. Geophys. Res.*, *110*, D08107, doi:10.1029/2004JD005516.

Fujiwara, M., K. Kita, and T. Ogawa (1998), Stratosphere-troposphere exchange of ozone associated with the equatorial Kelvin wave as observed with ozonesondes and rawinsondes, *J. Geophys. Res.*, *103*, 19,173–19,182.

Fujiwara, M., F. Hasebe, M. Shiotani, N. Nishi, H. Vömel, and S. J. Oltmans (2001), Water vapor control at the tropopause by equatorial Kelvin waves observed over the Galápagos, *Geophys. Res. Lett.*, *28*, 3143–3146.

Fujiwara, M., M. K. Yamamoto, H. Hashiguchi, T. Horinouchi, and S. Fukao (2003), Turbulence at the tropopause due to breaking Kelvin waves observed by the Equatorial Atmosphere Radar, *Geophys. Res. Lett.*, *30*(4), 1171, doi:10.1029/2002GL016278.

Gao, R. S., et al. (2004), Evidence that nitric acid increases relative humidity in low-temperature cirrus clouds, *Science*, *303*(5657), 516–520.

Garrett, T. J., A. J. Heymsfield, M. J. McGill, B. A. Ridley, D. G. Baumgardner, T. P. Bui, and C. R. Webster (2004), Convective generation of cirrus near the tropopause, *J. Geophys. Res.*, *109*, D21203, doi:10.1029/2004JD004952.

Gettelman, A., and P. M. de F. Forster (2002), A climatology of the tropical tropopause layer, *J. Meteorol. Soc. Jpn.*, *80*, 911–942.

Gettelman, A., and C. R. Webster (2005), Simulations of water isotope abundances in the upper troposphere and lower stratosphere and implications for stratosphere troposphere exchange, *J. Geophys. Res.*, *110*, D17301, doi:10.1029/2004JD004812.

Gettelman, A., W. J. Randel, S. Massie, F. Wu, W. G. Read, and J. M. Russell III (2001), El Niño as a natural experiment for studying the tropical tropopause region, *J. Clim.*, *14*, 3375–3392.

Gettelman, A., W. J. Randel, F. Wu, and S. T. Massie (2002a), Transport of water vapor in the tropical tropopause layer, *Geophys. Res. Lett.*, *29*(1), 1009, doi:10.1029/2001GL013818.

Gettelman, A. E., M. L. Salby, and F. Sassi (2002b), Distribution and influence of convection in the tropical tropopause region, *J. Geophys. Res.*, *107*(D10), 4080, doi:10.1029/2001JD001048.

Gettelman, A., P. M. de F. Forster, M. Fujiwara, Q. Fu, H. Vömel, L. K. Gohar, C. Johanson, and M. Ammerman (2004a), Radiation balance of the tropical tropopause layer, *J. Geophys. Res.*, *109*, D07103, doi:10.1029/2003JD004190.

Gettelman, A., D. E. Kinnison, T. J. Dunkerton, and G. P. Brasseur (2004b), Impact of monsoon circulation on the upper troposphere and lower stratosphere, *J. Geophys. Res.*, *109*, D22101, doi:10.1029/2004JD004878.

Gill, A. E. (1980), Some simple solutions for heat induced tropical circulation, *Q. J. R. Meteorol. Soc.*, *106*, 447–462.

Giorgetta, M. A., and L. Bengtsson (1999), Potential role of the quasi-biennial oscillation in the stratosphere-troposphere exchange as found in water vapor in general circulation model experiments, *J. Geophys. Res.*, *104*, 6003–6019.

Grosvenor, D. P., T. W. Choularton, H. Coe, and G. Held (2007), A study of the effect of overshooting deep convection on the water content of the TTL and lower stratosphere from Cloud Resolving Model simulations, *Atmos. Chem. Phys.*, *7*, 4977–5002.

Gunson, M. R., et al. (1996), The Atmospheric Trace Molecule Spectroscopy (ATMOS) experiment: Deployment on the ATLAS Space Shuttle mission, *Geophys. Res. Lett.*, *23*, 2333–2336.

Hartmann, D. L., J. R. Holton, and Q. Fu (2001), The heat balance of the tropical tropopause, cirrus, and stratospheric dehydration, *Geophys. Res. Lett.*, *28*, 1969–1972.

Hatsushika, H., and K. Yamazaki (2003), Stratospheric drain over Indonesia and dehydration within the tropical tropopause layer diagnosed by air parcel trajectories, *J. Geophys. Res.*, *108*(D19), 4610, doi:10.1029/2002JD002986.

Haynes, P. (2005), Stratospheric dynamics, *Annu. Rev. Fluid Mech.*, *37*, 263–293.

Haynes, P. H., and E. Shuckburgh (2000), Effective diffusivity as a diagnostic of atmospheric transport: 2. Troposphere and lower stratosphere, *J. Geophys. Res.*, *105*(D18), 22,795–22,810.

Haynes, P. H., C. J. Marks, M. E. McIntyre, T. G. Shepherd, and K. P. Shine (1991), On the "downward control" of extratropical diabatic circulations by eddy-induced mean zonal forces, *J. Atmos. Sci.*, *48*(4), 651–678.

Held, I. M. (1982), On the height of the tropopause and the static stability of the troposphere, *J. Atmos. Sci.*, *39*(2), 412–417.

Held, I. M., and A. Y. Hou (1980), Nonlinear axially symmetric circulations in a nearly inviscid atmosphere, *J. Atmos. Sci.*, *37*, 515–533.

Hervig, M., and M. McHugh (1999), Cirrus detection using HALOE measurements, *Geophys. Res. Lett.*, *26*, 719–722.

Highwood, E. J., and B. J. Hoskins (1998), The tropical tropopause, *Q. J. R. Meteorol. Soc.*, *124*, 1579–1604.

Hintsa, E. J., E. M. Weinstock, A. E. Dessler, J. G. Anderson, M. Loewenstein, and J. R. Podolske (1994), SPADE H_2O measurements and the seasonal cycle of stratospheric water vapor, *Geophys. Res. Lett.*, *21*, 2559–2562.

Hitchman, M. H., M. L. Buker, G. J. Tripoli, R. B. Pierce, J. A. Al-Saadi, E. V. Browell, and M. A. Avery (2004), A modeling study of an East Asian convective complex during March 2001, *J. Geophys. Res.*, *109*, D15S14, doi:10.1029/2003JD004312.

Hollars, S., Q. Fu, J. Comstock, and T. Ackerman (2004), Comparison of cloud-top height retrievals from ground-based 35 GHz MMCR and GMS-5 satellite observations at ARM TWP Manus site, *Atmos. Res.*, *72*, 169–186.

Holloway, C. E., and J. D. Neelin (2007), The convective cold top and quasi equilibrium, *J. Atmos. Sci.*, *64*, 1467–1487.

Holton, J. R., and A. Gettelman (2001), Horizontal transport and the dehydration of the stratosphere, *Geophys. Res. Lett.*, *28*, 2799–2802.

Holton, J. R., P. H. Haynes, M. E. McIntyre, A. R. Douglass, R. B. Rood, and L. Pfister (1995), Stratosphere-troposphere exchange, *Rev. Geophys.*, *33*, 403–440.

Holton, J. R., M. J. Alexander, and M. T. Boehm (2001), Evidence for short vertical wavelength Kelvin waves in the Department of Energy-Atmospheric Radiation Measurement Nauru99 radiosonde data, *J. Geophys. Res.*, *106*, 20,125–20,129.

Hong, G., G. Heygster, and K. Kunzi (2005), Intercomparison of deep convective cloud fractions from passive infrared and microwave radiance measurements, *IEEE Geosci. Remote Sens. Lett.*, *2*(1), 18–22.

Horinouchi, T., F. Sassi, and B. A. Boville (2000), Synoptic-scale Rossby waves and the geographic distribution of lateral transport routes between the tropics and the extratropics in the lower stratosphere, *J. Geophys. Res.*, *105*(D21), 26,579–26,592.

Houze, R. A., Jr. (1989), Observed structure of mesoscale convective systems and implications for large-scale heating, *Q. J. R. Meteorol. Soc.*, *115*(487), 425–461.

Immler, F., and O. Schrems (2002), Determination of tropical cirrus properties by simultaneous LIDAR and radiosonde measurements, *Geophys. Res. Lett.*, *29*(23), 2090, doi:10.1029/2002GL015076.

Jacob, D. J., et al. (1996), Origin of ozone and NOx in the tropical troposphere: A photochemical analysis of aircraft observations over the South Atlantic basin, *J. Geophys. Res.*, *101*, 24,235–24,520.

Jaegle, L., et al. (1997), Observations of OH and HO_2 in the upper troposphere suggest a strong source from convective injection of peroxides, *Geophys. Res. Lett.*, *24*, 3181–3184.

James, R., M. Bonazzola, B. Legras, K. Surbled, and S. Fueglistaler (2008), Water vapor transport and dehydration above convective outflow during Asian monsoon, *Geophys. Res. Lett.*, *35*, L20810, doi:10.1029/2008GL035441.

Jensen, E., and L. Pfister (2004), Transport and freeze-drying in the tropical tropopause layer, *J. Geophys. Res.*, *109*, D02207, doi:10.1029/2003JD004022.

Jensen, E., and L. Pfister (2005), Implications of persistent ice supersaturation in cold cirrus for stratospheric water vapor, *Geophys. Res. Lett.*, *32*, L01808, doi:10.1029/2004GL021125.

Jensen, E. J., O. B. Toon, L. Pfister, and H. B. Selkirk (1996a), Dehydration of the upper troposphere and lower stratosphere by subvisible cirrus clouds near the tropical tropopause, *Geophys. Res. Lett.*, *23*, 825–828.

Jensen, E. J., O. B. Toon, H. B. Selkirk, J. D. Spinhirne, and M. R. Schoeberl (1996b), On the formation and persistence of subvisible cirrus clouds near the tropical tropopause, *J. Geophys. Res.*, *101*, 21,361–21,375.

Jensen, E. J., L. Pfister, A. Ackerman, O. B. Toon, and A. Tabazadeh (2001), A conceptual model of the dehydration of air due to freeze-drying by optically thin, laminar cirrus rising slowly across the tropical tropopause, *J. Geophys. Res.*, *106*, 17,237–17,252.

Jensen, E. J., et al. (2005a), Ice supersaturations exceeding 100% at the cold tropical tropopause: Implications for cirrus formation and dehydration, *Atmos. Chem. Phys.*, *5*, 851–862.

Jensen, E., L. Pfister, T. Bui, A. Weinheimer, E. Weinstock, J. Smith, J. Pittman, D. Baumgardner, P. Lawson, and M. J. McGill (2005b), Formation of a tropopause cirrus layer observed over Florida during CRYSTAL-FACE, *J. Geophys. Res.*, *110*, D03208, doi:10.1029/2004JD004671.

Jensen, E. J., A. S. Ackerman, and J. A. Smith (2007), Can overshooting convection dehydrate the tropical tropopause layer?, *J. Geophys. Res.*, *112*, D11209, doi:10.1029/2006JD007943.

Jin, F. F., and B. J. Hoskins (1995), The direct response to tropical heating in a baroclinic atmosphere, *J. Atmos. Sci.*, *52*(3), 307–319.

Jing, P., D. M. Cunnold, H. J. Wang, and E. S. Yang (2004), Isentropic cross-tropopause ozone transport in the Northern Hemisphere, *J. Atmos. Sci.*, *61*, 1068–1078.

Johnson, D. G., K. W. Jucks, W. A. Traub, and K. V. Chance (2001), Isotopic composition of stratospheric water vapor: Measurements and photochemistry, *J. Geophys. Res.*, *106*(D11), 12,211–12,217.

Johnson, R. H., and D. C. Kriete (1982), Thermodynamic and circulation characteristics of winter monsoon tropical mesoscale convection, *Mon. Weather Rev.*, *110*, 1898–1911.

Johnston, H. S., and S. Solomon (1979), Thunderstorms as possible micrometeorological sink for stratospheric water, *J. Geophys. Res.*, *84*(6), 3155–3158.

Jorgensen, D. P., and M. A. LeMone (1989), Vertical velocity characteristics of oceanic convection, *J. Atmos. Sci.*, *46*(5), 621–640.

Kahn, B. H., K. N. Liou, S.-Y. Lee, E. F. Fishbein, S. DeSouza-Machado, A. Eldering, E. J. Fetzer, S. E. Hannon, and L. L. Strow (2005), Nighttime cirrus detection using Atmospheric Infrared Sounder window channels and total column water vapor, *J. Geophys. Res.*, *110*, D07203, doi:10.1029/2004JD005430.

Katagiri, S., and T. Nakajima (2004), Radiative characteristics of cirrus clouds as retrieved from AVHRR, *J. Meteorol. Soc. Jpn.*, *82*, 81–99.

Keim, E. R., et al. (1999), NO_y partitioning from measurements of nitrogen and hydrogen radicals in the upper troposphere, *Geophys. Res. Lett.*, *26*(1), 51–54.

Kerr-Munslow, A. M., and W. A. Norton (2006), Tropical, wave driving of the annual cycle in tropical tropopause temperatures. Part I: ECMWF analyses, *J. Atmos. Sci.*, *63*(5), 1410–1419.

Kiehl, J. T., and S. Solomon (1986), On the radiative balance of the stratosphere, *J. Atmos. Sci.*, *43*, 1525–1534.

Kiladis, G. N., K. H. Straub, G. C. Reid, and K. S. Gage (2001), Aspects of interannual and intraseasonal variability of the tropopause and lower stratosphere, *Q. J. R. Meteorol. Soc.*, *127*, 1961–1983.

Kley, D., E. J. Stone, W. R. Henderson, J. W. Drummond, W. J. Harrop, A. L. Schmeltekopf, T. L. Thompson, and R. H. Winkler (1979), In situ measurements of the mixing ratio of water vapor in the stratosphere, *J. Atmos. Sci.*, *36*, 2513–2524.

Kley, D., et al. (2000), SPARC assessment of upper tropospheric and stratospheric water vapour, *WCRP 113*, World Meteorol. Organ., Geneva, Switzerland.

Kritz, M. A., S. W. Rosner, K. K. Kelly, M. Lewenstein, and K. R. Chan (1993), Radon measurements in the lower tropical stratosphere: Evidence for rapid vertical transport and dehydration of tropospheric air, *J. Geophys. Res.*, *98*, 8725–8736.

Kuang, Z. M., and C. S. Bretherton (2004), Convective influence on the heat balance of the tropical tropopause layer: A cloud-resolving model study, *J. Atmos. Sci.*, *23*, 2919–2927.

Kuang, Z., G. C. Toon, P. O. Wennberg, and Y. L. Yung (2003), Measured HDO/H_2O ratios across the tropical tropopause, *Geophys. Res. Lett.*, *30*(7), 1372, doi:10.1029/2003GL017023.

Küpper, C., J. Thuburn, G. C. Craig, and T. Birner (2004), Mass and water transport into the tropical stratosphere: A cloud-resolving simulation, *J. Geophys. Res.*, *109*, D10111, doi:10.1029/2004JD004541.

Lanzante, J. R., S. A. Klein, and D. J. Seidel (2003), Temporal homogenization of monthly radiosonde temperature data. Part II: Trends, sensitivities, and MSU comparison, *J. Clim.*, *16*, 241–262.

Lawrence, M. G., P. J. Crutzen, and P. J. Rasch (1999), Analysis of the CEPEX ozone data using a 3D chemistry-meteorology model, *Q. J. R. Meteorol. Soc.*, *125*, 2987–3009.

Liu, C., and E. J. Zipser (2005), Global distribution of convection penetrating the tropical tropopause, *J. Geophys. Res.*, *110*, D23104, doi:10.1029/2005JD006063.

Logan, J. A. (1999), An analysis of ozonesonde data for the troposphere: Recommendations for testing 3-D models and development of a gridded climatology for tropospheric ozone, *J. Geophys. Res.*, *104*(D13), 16,115–16,149.

Luo, B. P., et al. (2003), Ultrathin tropical tropopause clouds (UTTCs): II. Stabilization and destabilization mechanism, *Atmos. Chem. Phys.*, *3*, 1093–1100.

Luo, Z., and W. B. Rossow (2004), Characterizing tropical cirrus life cycle, evolution, and interaction with upper-tropospheric water vapor using Lagrangian trajectory analysis of satellite observations, *J. Clim.*, *17*, 4541–4563.

Madden, R. A., and P. R. Julian (1971), Detection of a 40–50 day oscillation in zonal wind in the tropical Pacific, *J. Atmos. Sci.*, *28*(5), 702–708.

Madden, R. A., and P. R. Julian (1994), Observations of the 40–50 day tropical oscillation—A review, *Mon. Weather Rev.*, *122*, 814–837.

Manabe, S., and R. F. Strickler (1964), Thermal equilibrium of the Atmosphere with a convective adjustment, *J. Atmos. Sci.*, *21*(4), 361–385.

Marcy, T. P., et al. (2007), Measurements of trace gases in the tropical tropopause layer, *Atmos. Environ.*, *41*(34), 7253–7261, doi:10.1016/j.atmosenv.2007.05.032.

Massie, S., A. Gettelman, W. Randel, and D. Baumgardner (2002), Distribution of tropical cirrus in relation to convection, *J. Geophys. Res.*, *107*(D21), 4591, doi:10.1029/2001JD001293.

Matsuno, T. (1966), Quasi-geostrophic motions in the equatorial area, *J. Meteorol. Soc. Jpn.*, *44*, 25–43.

McCarthy, M. C., K. A. Boering, T. Rahn, J. M. Eiler, A. L. Rice, S. C. Tyler, S. Schauffler, E. Atlas, and D. G. Johnson (2004), The hydrogen isotopic composition of water vapor entering the stratosphere inferred from high precision measurements of δD-CH_4 and δD-H_2, *J. Geophys. Res.*, *109*, D07304, doi:10.1029/2003JD004003.

McCormick, M. P., et al. (1993), Annual variations in water vapor in the stratosphere and upper troposphere observed by the Stratospheric Aerosol and Gas Experiement II, *J. Geophys. Res.*, *98*, 4867–4874.

McFarquhar, G. M., A. J. Heymsfield, J. Spinhirne, and B. Hart (2000), Thin and subvisual tropopause tropical cirrus: Observations and radiative impacts, *J. Atmos. Sci.*, *57*(12), 1841–1853.

McIntyre, M. E., and T. N. Palmer (1984), The surf zone in the stratosphere, *J. Atmos. Terr. Phys.*, *46*(9), 825–849.

Michelsen, H. A., F. W. Irion, G. L. Manney, G. C. Toon, and M. R. Gunson (2000), Features and trends in Atmospheric Trace Molecule Spectroscopy (ATMOS) version 3 stratospheric water vapor and methane measurements, *J. Geophys. Res.*, *105*, 22,713–22,724.

Minschwaner, K., A. E. Dessler, J. W. Elkins, C. M. Volk, D. W. Fahey, M. Loewenstein, J. R. Podolske, A. E. Roche, and K. R. Chan (1996), Bulk properties of isentropic mixing into the tropics in the lower stratosphere, *J. Geophys. Res.*, *101*, 9433–9439.

Mote, P. W., and R. Frey (2006), Variability of clouds and water vapor in low latitudes: View from Moderate Resolution Imaging Spectroradiometer (MODIS), *J. Geophys. Res.*, *111*, D16101, doi:10.1029/2005JD006791.

Mote, P. W., K. H. Rosenlof, J. R. Holton, R. S. Harwood, and J. W. Waters (1995), Seasonal variations of water vapor in the tropical lower stratosphere, *Geophys. Res. Lett.*, *22*(9), 1093–1096.

Mote, P. W., K. H. Rosenlof, M. E. McIntyre, E. S. Carr, J. C. Gille, J. R. Holton, J. S. Kinnersley, and H. C. Pumphrey (1996), An atmospheric tape recorder: The imprint of tropical tropopause temperatures on stratospheric water vapor, *J. Geophys. Res.*, *101*, 3989–4006.

Mote, P. W., H. L. Clark, T. J. Dunkerton, R. S. Harwood, and H. C. Pumphrey (2000), Intraseasonal variations of water vapor in the tropical upper troposphere and tropopause region, *J. Geophys. Res.*, *105*(D13), 17,457–17,470.

Moyer, E. J., F. W. Irion, Y. L. Yung, and M. R. Gunson (1996), ATMOS stratospheric deuterated water and implications for troposphere-stratosphere transport, *Geophys. Res. Lett.*, *23*, 2385–2388.

Murphy, D. M. (2003), Dehydration in cold clouds is enhanced by a transition from cubic to hexagonal ice, *Geophys. Res. Lett.*, *30*(23), 2230, doi:10.1029/2003GL018566.

Neelin, J. D., and I. M. Held (1987), Modelling tropical convergence based on the moist static energy budget, *Mon. Weather Rev.*, *115*, 3–12.

Newell, R. E., and S. Gould-Stewart (1981), A stratospheric fountain?, *J. Atmos. Sci.*, *38*, 2789–2796.

Newell, R. E., Y. Zhu, E. V. Browell, W. G. Read, and J. W. Waters (1996), Walker circulation and tropical upper tropospheric water vapor, *J. Geophys. Res.*, *101*, 1961–1974.

Newman, P. A., and J. E. Rosenfield (1997), Stratospheric thermal damping times, *Geophys. Res. Lett.*, *24*, 433–436.

Niwano, M., K. Yamazaki, and M. Shiotani (2003), Seasonal and QBO variations of ascent rate in the tropical lower stratosphere as inferred from UARS HALOE trace gas data, *J. Geophys. Res.*, *108*(D24), 4794, doi:10.1029/2003JD003871.

Norton, W. A. (2006), Tropical wave driving of the annual cycle in tropical tropopause temperatures, part II: Model results, *J. Atmos. Sci.*, *63*, 1420–1431.

Notholt, J., et al. (2003), Enhanced upper tropical tropospheric COS: Impact on the stratospheric aerosol layer, *Science*, *300*, 307–310.

Notholt, J., et al. (2005), Influence of tropospheric SO_2 emissions on particle formation and the stratospheric humidity, *Geophys. Res. Lett.*, *32*, L07810, doi:10.1029/2004GL022159.

Oltmans, S. J., H. Vömel, D. J. Hofmann, K. H. Rosenlof, and D. Kley (2000), The increase in stratospheric water vapor from ballonborne, frostpoint hygrometer measurements at Washington, D.C., and Boulder, Colorado, *Geophys. Res. Lett.*, *27*, 3453–3456.

Park, M., W. J. Randel, D. E. Kinnison, R. R. Garcia, and W. Choi (2004), Seasonal variation of methane, water vapor and nitrogen oxides near the tropopause: Satellite observations and model simulation, *J. Geophys. Res.*, *109*, D03302, doi:10.1029/2003JD003706.

Park, M., W. J. Randel, L. K. Emmons, P. F. Bernath, K. A. Walker, and C. D. Boone (2008), Chemical isolation in the Asian monsoon anticyclone observed in Atmospheric Chemistry Experiment (ACE-FTS) data, *Atmos. Chem. Phys.*, *8*, 757–764.

Park, S., et al. (2007), The CO_2 tracer clock for the tropical tropopause layer, *Atmos. Chem. Phys.*, *7*, 3989–4000.

Peter, T., et al. (2003), Ultrathin tropical tropopause clouds (UTTCs): I. Cloud morphology and occurrence, *Atmos. Chem. Phys.*, *3*, 1083–1091.

Peter, T., M. Krämer, and O. Möhler (2008), Upper tropospheric humidity: A report on an international workshop, *SPARC Newsl.*, *30*, 9–15.

Pfister, L., et al. (2001), Aircraft observations of thin cirrus clouds near the tropical tropopause, *J. Geophys. Res.*, *106*(D9), 9765–9786.

Plumb, R. A. (1996), A "tropical pipe" model of stratospheric transport, *J. Geophys. Res.*, *101*(D2), 3957–3972.

Plumb, R. A. (2002), Stratospheric transport, *J. Meteorol. Soc. Jpn.*, *80*, 793–801.

Plumb, R. A., and J. Eluszkiewicz (1999), The Brewer-Dobson circulation: Dynamics of the tropical upwelling, *J. Atmos. Sci.*, *56*, 868–890.

Polvani, L. M., D. W. Waugh, and R. A. Plumb (1995), On the subtropical edge of the stratospheric surf zone, *J. Atmos. Sci.*, *52*(9), 1288–1309.

Popp, P. J., et al. (2004), Nitric acid uptake on subtropical cirrus cloud particles, *J. Geophys. Res.*, *109*, D06302, doi:10.1029/2003JD004255.

Popp, P. J., et al. (2006), The observation of nitric acid-containing particles in the tropical lower stratosphere, *Atmos. Chem. Phys.*, *6*, 601–611.

Potter, B. E., and J. R. Holton (1995), The role of monsoon convection in the dehydration of the lower tropical stratosphere, *J. Atmos. Sci.*, *38*, 1034–1050.

Ramaswamy, V., et al. (2001), Stratospheric temperature trends: Observations and model simulations, *Rev. Geophys.*, *39*(1), 71–122.

Randel, W. J., and M. Park (2006), Deep convective influence on the Asian summer monsoon anticyclone and associated tracer variability observed with Atmospheric Infrared Sounder (AIRS), *J. Geophys. Res.*, *111*, D12314, doi:10.1029/2005JD006490.

Randel, W. J., and F. Wu (2005), Kelvin wave variability near the equatorial tropopause observed in GPS radio occultation measurements, *J. Geophys. Res.*, *110*, D03102, doi:10.1029/2004JD005006.

Randel, W. J., F. Wu, J. M. Russell III, A. Roche, and J. W. Waters (1998), Seasonal cycles and QBO variations in stratospheric CH_4 and H_2O observed in UARS HALOE data, *J. Atmos. Sci.*, *55*, 163–185.

Randel, W. J., F. Wu, and D. J. Gaffen (2000), Interannnual variability of the tropical tropopause derived from radiosonde data and NCEP reanalyses, *J. Geophys. Res.*, *105*(D12), 15,509–15,523.

Randel, W. J., F. Wu, A. Gettelman, J. M. Russell III, J. M. Zawodny, and S. J. Oltmans (2001), Seasonal variation of water vapor in the lower stratosphere observed in Halogen Occultation Experiment data, *J. Geophys. Res.*, *106*, 14,313–14,325.

Randel, W. J., R. R. Garcia, and F. Wu (2002), Time-dependent upwelling in the tropical lower stratosphere estimated from the zonal-mean momentum budget, *J. Atmos. Sci.*, *59*, 2141–2152.

Randel, W. J., F. Wu, S. J. Oltmans, K. Rosenlof, and G. E. Nedoluha (2004), Interannual changes of stratospheric water vapor and correlations with tropical tropopause temperatures, *J. Atmos. Sci.*, *61*, 2133–2148.

Randel, W. J., F. Wu, H. Vömel, G. E. Nedoluha, and P. Forster (2006), Decreases in stratospheric water vapor after 2001: Links to changes in the tropical tropopause and the Brewer-Dobson circulation, *J. Geophys. Res.*, *111*, D12312, doi:10.1029/2005JD006744.

Randel, W. J., M. Park, F. Wu, and N. Livesey (2007), A large annual cycle in ozone above the tropical tropopause linked to the Brewer-Dobson circulation, *J. Atmos. Sci.*, *64*(12), 4479–4488.

Randel, W. J., R. Garcia, and F. Wu (2008), Dynamical balances and tropical stratospheric upwelling, *J. Atmos. Sci.*, *65*(11), 3584–3595.

Raymond, D. J. (1995), Regulation of moist convection over the West Pacific Warm Pool, *J. Atmos. Sci.*, *52*(22), 3945–3959.

Read, W. G., D. L. Wu, J. W. Waters, and H. C. Pumphrey (2004), A new 137–56 hPa water vapor product from the UARS Microwave Limb Sounder, *J. Geophys. Res.*, *109*, D06111, doi:10.1029/2003JD004366.

Read, W. G., et al. (2007), Aura Microwave Limb Sounder upper tropospheric and lower stratospheric H_2O and relative humidity with respect to ice validation, *J. Geophys. Res.*, *112*, D24S35, doi:10.1029/2007JD008752.

Reed, R. J. (1962), Some features of the annual temperature regime in the tropical stratosphere, *Mon. Weather Rev.*, *90*(6), 211–215.

Reed, R. J., and C. L. Vlcek (1969), The annual temperature variation in the lower tropical stratosphere, *J. Amtos. Sci.*, *26*, 163–167.

Reid, G. C., and K. S. Gage (1981), On the annual variation in height of the tropical tropopause, *J. Atmos. Sci.*, *38*, 1928–1938.

Reid, G. C., and K. S. Gage (1996), The tropical tropopause over the western Pacific: Wave driving, convection, and the annual cycle, *J. Geophys. Res.*, *101*, 21,233–21,241.

Ridley, B., et al. (2004), Convective transport of reactive constituents to the tropical and mid-latitude tropopause region: I. Observations, *Atmos. Environ.*, *38*(9), 1259–1274.

Robinson, F. J., and S. C. Sherwood (2006), Modeling the impact of convective entrainment on the tropical tropopause, *J. Atmos. Sci.*, *63*, 1013–1027.

Robinson, G. D. (1980), The transport of minor atmospheric constituents between troposphere and stratosphere, *Q. J. R. Meteorol. Soc.*, *106*, 227–253.

Rosenfield, J. E., D. B. Considine, M. R. Schoeberl, and E. V. Browell (1998), The impact of subvisible cirrus clouds near the tropical tropopause on stratospheric water vapor, *Geophys. Res. Lett.*, *25*, 1883–1886.

Rosenlof, K. H. (1995), Seasonal cycle of the residual mean meridional circulation in the stratosphere, *J. Geophys. Res.*, *100*(D3), 5173–5191.

Rosenlof, K. H., et al. (2001), Stratospheric water vapor increases over the past half-century, *Geophys. Res. Lett.*, *28*, 1195–1198.

Rossow, W. B., and C. Pearl (2007), 22-year survey of tropical convection penetrating into the lower stratosphere, *Geophys. Res. Lett.*, *34*, L04803, doi:10.1029/2006GL028635.

Russell, J. M., III, L. L. Gordley, J. H. Park, S. R. Drayson, W. D. Hesketh, R. J. Cicerone, A. F. Tuck, J. E. Frederick, J. E. Harries, and P. J. Crutzen (1993), The Halogen Occultation Experiment, *J. Geophys. Res.*, *98*, 10,777–10,798.

Salawitch, R. J., D. K. Weisenstein, L. J. Kovalenko, C. E. Sioris, P. O. Wennberg, K. Chance, M. K. W. Ko, and C. A. McLinden (2005), Sensitivity of ozone to bromine in the lower stratosphere, *Geophys. Res. Lett.*, *32*, L05811, doi:10.1029/2004GL021504.

Sandor, B. J., E. J. Jensen, E. M. Stone, W. G. Read, J. W. Waters, and J. L. Mergenthaler (2000), Upper tropospheric humidity and thin cirrus, *Geophys. Res. Lett.*, *27*, 2645–2648.

Sardeshmukh, P. D., and B. J. Hoskins (1988), The generation of global rotational flow by steady idealized tropical divergence, *J. Atmos. Sci.*, *45*(7), 1228–1251.

Sassen, K., and B. S. Cho (1992), Subvisual-thin cirrus clouds lidar data set for satellite verification and climatological research, *J. Appl. Meteorol.*, *31*, 1275–1285.

Scaife, A. A., N. Butchart, D. R. Jackson, and R. Swinbank (2003), Can changes in ENSO activity help to explain increasing stratospheric water vapor?, *Geophys. Res. Lett.*, *30*(17), 1880, doi:10.1029/2003GL017591.

Scherer, M., H. Vömel, S. Fueglistaler, S. J. Oltmans, and J. Staehelin (2008), Trends and variability of midlatitude stratospheric water vapour deduced from the re-evaluated Boulder balloon series and HALOE, *Atmos. Chem. Phys.*, *8*, 1391–1402.

Schmidt, T., J. Wickert, G. Beyerle, and C. Reigber (2004), Tropical tropopause parameters derived from GPS radio occultation measurements with CHAMP, *J. Geophys. Res.*, *109*, D13105, doi:10.1029/2004JD004566.

Schneider, R., and G. M. Barnes (2005), Low-level kinematic, thermodynamic, and reflectivity fields associated with Hurricane Bonnie (1998) at landfall, *Mon. Weather Rev.*, *133*, 3243–3260.

Schoeberl, M. R., B. N. Duncan, A. R. Douglass, J. Waters, N. Livesey, W. Read, and M. Filipiak (2006), The carbon monoxide tape recorder, *Geophys. Res. Lett.*, *33*, L12811, doi:10.1029/2006GL026178.

Scott, R. K. (2002), Wave-driven mean tropical upwelling in the lower stratosphere, *J. Atmos. Sci.*, *59*, 2745–2759.

Seidel, D. J., R. J. Ross, J. K. Angell, and G. C. Reid (2001), Climatological characteristics of the tropical tropopause as revealed by radiosondes, *J. Geophys. Res.*, *106*, 7857–7878.

Selkirk, H. B. (1993), The tropopause cold trap in the Australian monsoon during STEP/AMEX 1987, *J. Geophys. Res.*, *98*, 8591–8610.

Semeniuk, K., and T. G. Shepherd (2001), Mechanisms for tropical upwelling in the stratosphere, *J. Atmos. Sci.*, *58*, 3097–3115.

Sherwood, S. C. (1999), On moistening of the tropical troposphere by cirrus clouds, *J. Geophys. Res.*, *104*, 11,949–11,960.

Sherwood, S. C. (2000), A stratospheric "drain" over the maritime continent, *Geophys. Res. Lett.*, *27*, 677–680.

Sherwood, S. C. (2002), A microphysical connection among biomass burning, cumulus clouds, and stratospheric moisture, *Science*, *295*, 1272–1275.

Sherwood, S. C., and A. E. Dessler (2000), On the control of stratospheric humidity, *Geophys. Res. Lett.*, *27*, 2513–2516.

Sherwood, S. C., and A. E. Dessler (2003), Convective mixing near the tropical tropopause: Insights from seasonal variations, *J. Atmos. Sci.*, 2674–2685.

Sherwood, S. C., T. Horinouchi, and H. A. Zeleznik (2003), Convective impact on temperatures observed near the tropical tropopause, *J. Atmos. Sci.*, *60*, 1847–1856.

Sherwood, S. C., J.-H. Chae, P. Minnis, and M. McGill (2004), Underestimation of deep convective cloud tops by thermal imagery, *Geophys. Res. Lett.*, *31*, L11102, doi:10.1029/2004GL019699.

Sherwood, S. C., E. R. Kursinsky, and W. G. Read (2006), A distribution law for free-tropospheric relative humidity, *J. Clim.*, *19, 6267–6277.*

Shimizu, A., and T. Tsuda (1997), Characteristics of Kelvin waves and gravity waves observed with radiosondes over Indonesia, *J. Geophys. Res.*, *102*, 26,159–26,172.

Shiotani, M. (1992), Annual, quasi-biennial and El-Nino-Southern Oscillation (ENSO) time-scale variations in equatorial total ozone, *J. Geophys. Res.*, *97*, 7625–7634.

Simmons, A., S. Uppala, D. Dee, and S. Kobayashi (2006), ERA-Interim: New ECMWF reanalysis products from 1989 onwards, *ECMWF Newsl.*, *110*, 25–35.

Sinnhuber, B.-M., and I. Folkins (2006), Estimating the contribution of bromoform to stratospheric bromine and its relation to dehydration in the tropical tropopause layer, *Atmos. Chem. Phys.*, *6*, 4755–4761.

Smith, J. A., A. S. Ackerman, E. J. Jensen, and O. B. Toon (2006), Role of deep convection in establishing the isotopic composition of water vapor in the tropical transition layer, *Geophys. Res. Lett.*, *33*, L06812, doi:10.1029/2005GL024078.

Solomon, S., R. R. Garcia, F. S. Rowland, and D. J. Wuebles (1986), On the depletion of Antarctic ozone, *Nature*, *321*, 755–758.

Spang, R., G. Eidmann, M. Riese, D. Offermann, P. Preusse, L. Pfister, and P.-H. Wang (2002), CRISTA observations of cirrus clouds around the tropopause, *J. Geophys. Res.*, *107*(D23), 8174, doi:10.1029/2001JD000698.

Strahan, S. E., A. R. Douglass, J. E. Nielsen, and K. A. Boering (1998), The CO_2 seasonal cycle as a tracer for transport, *J. Geophys. Res.*, *103*(D12), 13,729–13,741.

Thompson, A. M., et al. (2003a), Southern Hemisphere Additional Ozonesondes (SHADOZ) 1998–2000 tropical ozone climatology 1. Comparison with Total Ozone Mapping Spectrometer

(TOMS) and ground-based measurements, *J. Geophys. Res.*, *108*(D2), 8238, doi:10.1029/2001JD000967.

Thompson, A. M., et al. (2003b), Southern Hemisphere Additional Ozonesondes (SHADOZ) 1998–2000 tropical ozone climatology 2. Tropospheric variability and the zonal wave-one, *J. Geophys. Res.*, *108*(D2), 8241, doi:10.1029/2002JD002241.

Thuburn, J., and G. C. Craig (2000), Stratospheric influence on tropopause height: The radiative constraint, *J. Atmos. Sci.*, *57*, 17–28.

Thuburn, J., and G. C. Craig (2002), On the temperature structure of the tropical substratosphere, *J. Geophys. Res.*, *107*(D2), 4017, doi:10.1029/2001JD000448.

Tuck, A. F., S. J. Hovde, K. K. Kelly, M. J. Mahoney, M. H. Proffitt, E. C. Richard, and T. L. Thompson (2003), Exchange between the upper tropical troposphere and the lower stratosphere studied with aircraft observations, *J. Geophys. Res.*, *108*(D23), 4734, doi:10.1029/2003JD003399.

Tuck, A. F., et al. (2004), Horizontal variability 1–2 km below the tropical tropopause, *J. Geophys. Res.*, *109*, D05310, doi:10.1029/2003JD003942.

Uppala, S. M., et al. (2005), The ERA-40 re-analysis, *Q. J. R. Meteorol. Soc.*, *131*, 2961–3012.

Volk, C. M., et al. (1996), Quantifying transport between the tropical and mid-latitude lower stratosphere, *Science*, *272*(5269), 1763–1768.

Wallace, J. M., and V. E. Kousky (1968), Observational evidence of Kelvin waves in the tropical stratosphere, *J. Atmos. Sci.*, *25*(5), 900–907.

Wang, L. K., and A. E. Dessler (2006), Instantaneous cloud overlap statistics in the tropical area revealed by ICESat/GLAS data, *Geophys. Res. Lett.*, *33*, L15804, doi:10.1029/2005GL024350.

Wang, P.-H., P. Minnis, M. P. McCormick, G. S. Kent, and K. M. Skeens (1996), A 6-year climatology of cloud occurrence frequency from Stratospheric Aerosol and Gas Experiment II observations (1985–1990), *J. Geophys. Res.*, *101*(D23), 29,407–29,429.

Waugh, D. W., and B. M. Funatsu (2003), Intrusions into the tropical upper troposphere: Three-dimensional structure and accompanying ozone and OLR distributions, *J. Atmos. Sci.*, *60*, 637–653.

Waugh, D. W., and L. M. Polvani (2000), Climatology of intrusions into the tropical upper troposphere, *Geophys. Res. Lett.*, *27*, 3857–3860.

Webster, C. R., and A. J. Heymsfield (2003), Water isotope ratios D/H, O-18/O-16, O-17/O-16 in and out of clouds map dehydration pathways, *Science*, *302*(5651), 1742–1745.

Weickmann, K. M., and R. M. Chervin (1988), The observed and simulated atmospheric seasonal cycle: I. Global wind field modes, *J. Clim.*, *1*, 265–289.

Weinstock, E. M., E. J. Hintsa, A. E. Dessler, and J. G. Anderson (1995), Measurements of water vapor in the tropical lower stratosphere during the CEPEX campaign: Results and interpretation, *Geophys. Res. Lett.*, *22*, 3231–3234.

Wennberg, P. O., et al. (1998), Hydrogen radicals, nitrogen radicals, and the production of O_3 in the upper troposphere, *Science*, *279*, 49–53.

Winker, D. M., and C. R. Trepte (1998), Laminar cirrus observed near the tropical tropopause by LITE, *Geophys. Res. Lett.*, *25*, 3351–3354.

Winker, D. M., W. H. Hunt, and M. J. McGill (2007), Initial performance assessment of CALIOP, *Geophys. Res. Lett.*, *34*, L19803, doi:10.1029/2007GL030135.

Wong, S., and A. E. Dessler (2007), Regulation of H_2O and CO in tropical tropopause layer by the Madden-Julian oscillation, *J. Geophys. Res.*, *112*, D14305, doi:10.1029/2006JD007940.

Yulaeva, E., J. R. Holton, and J. M. Wallace (1994), On the cause of the annual cycle in tropical lower-stratospheric temperatures, *J. Atmos. Sci.*, *51*(2), 169–174.

Zachariasse, M., P. F. J. van Velthoven, H. G. J. Smit, J. Lelieveld, T. K. Mandal, and H. Kelder (2000), Influence of stratosphere-troposphere exchange on tropospheric ozone over the tropical Indian Ocean during the winter monsoon, *J. Geophys. Res.*, *105*(D12), 15,403–15,416.

Zhou, X.-L., and J. R. Holton (2002), Intraseasonal variations of tropical cold point temperatures, *J. Clim.*, *15*, 1460–1473.

Zhou, X. L., M. A. Geller, and M. Zhang (2001), Cooling trend of the tropical cold point tropopause temperatures and its implications, *J. Geophys. Res.*, *106*(D2), 1511–1522.

Zipser, E. J., D. J. Cecil, C. T. Liu, S. W. Nesbitt, and D. P. Yorti (2006), Where are the most intense thunderstorms on Earth?, *Bull. Am. Meteorol. Soc.*, *87*(8), 1057–1071.

A. E. Dessler, Department of Atmospheric Sciences, Texas A&M University, College Station, TX 77843, USA.

T. J. Dunkerton and P. W. Mote, NorthWest Research Associates, Redmond, WA 98052, USA.

I. Folkins, Department of Physics and Atmospheric Science, Dalhousie University, Halifax, NS B3H 3J5, Canada.

Q. Fu, Department of Atmospheric Sciences, University of Washington, Seattle, WA 98195, USA.

S. Fueglistaler, Department of Applied Mathematics and Theoretical Physics, University of Cambridge, Cambridge CB3 0WA, UK. (s.fueglistaler@damtp.cam.ac.uk)